chloroform as eluant. Analytical samples were prepared by further recrystallization in methanol/chloroform (1:2). The purified product was analyzed by ^{13}C NMR spectroscopy. All new compounds gave satisfactory elemental analysis (cf. Table I).

Acknowledgment. Support of our work by the National Institutes of Health is gratefully acknowledged.

Registry No. **1**, 768-92-3; **1** bromide, 768-90-1; **2**, 16668-83-0; **2** alcohol, 700-57-2; **3**, 54043-61-7; **3** chloride, 16104-50-0; **4**, 54043-62-8; **4** bromide, 707-34-6; **5**, 54043-63-9; **5** bromide, 7314-86-5; 6, 77052-09-6; 6 bromide, 30545-17-6; **7**, 77052-10-9; **7** alcohol, 30651-03-7; **8**, 90481-59-7; **8** alcohol, 30545-24-5; **9**, 90481-60-0; **9** bromide, 32401-10-8; **10**, 90481-61-1; **10** chloride, 32401-20-0; $NO_2^+BF^-$, 13826-86-3; PPHF, 62778-11-4.

Synthesis, Structural Characterization, and Electronic Structures of the "Mixed" Terminal Ligand Cubanes $[Fe_4S_4Cl_2(XC_6H_5)_2]^{2-}$ (X = S, O) and $[Fe_4S_4(SC_6H_5)_2(OC_6H_4\text{-}p\text{-}CH_3)_2]^{2-}$. The First Examples of $[Fe_4S_4]^{2+}$ Cores with a Noncompressed D_{2d} Idealized Geometry

M. G. Kanatzidis,[†] N. C. Baenziger,[†1] D. Coucouvanis,*[†] A. Simopoulos,[‡] and A. Kostikas[‡]

Contribution from the Department of Chemistry, University of Michigan, Ann Arbor, Michigan 48109, and Nuclear Research Center "Demokritos", Aghia Paraskevi, Attiki, Greece.
Received January 23, 1984

Abstract: Mixed terminal ligand iron-sulfur clusters of the type $(Ph_4P)_2[Fe_4S_4(L)_2(L')_2]$ (L = SPh, L' = Cl, OPh, Br; L = OPh, L' = Cl) have been synthesized in good yields by the reaction of $[Fe_4S_4X_4]^{2-}$ (X = Cl, Br) with 2 equiv of KSPh or NaOPh and by the reaction of $[Fe_4S_4(SPh)_2Cl_2]^{2-}$ with 2 equiv of NaOPh, respectively. The crystal structures of $(Ph_4P)_2[Fe_4S_4(XPh)_2Cl_2]$ (I, X = S; II, X = O) and $(Ph_4P)_2[Fe_4S_4(SPh)_2(OPh\text{-}p\text{-}CH_3)_2]$ (III) are described in detail. Crystalline salts of I and II show symmetry consistent with the orthorhombic space group *Pbcn* with cell a = 13.082 (1) Å, b = 21.182 (4) Å, and c = 21.376 (4) Å and a = 13.060 (3) Å, b = 20.891 (5) Å, and c = 21.423 (7) Å, respectively. Salt III belongs to the noncentrosymmetric orthorhombic space group $P2_12_12$ with cell constants a = 24.595 (7) Å, b = 12.588 (3) Å, and c = 10.877 (3) Å. In all structures all non-hydrogen atoms were refined anisotropically and hydrogen atoms were included in the structure factor calculation but not refined. Refinement by full-matrix least squares of 334 parameters on 2203 data for I, 334 parameters on 2149 data for II, and 397 parameters on 3231 data for III gave final R values of 0.061, 0.061, and 0.066, respectively. The anions in I and II are located on the crystallographically imposed twofold axis. The mean Fe-S* bond lengths in I and II are 2.278 (5) and 2.285 (5) Å, respectively. The Fe_4S_4* cores in I and II represent the first examples of such cores without an overall compressed D_{2d} geometry. The anion in III also is located on a crystallographic twofold axis. The Fe_4S_4* unit can be described as slightly compressed along an axis that is perpendicular to the crystallographic twofold. The terminal Fe-SPh bond lengths in I and III are 2.261 (3) and 2.289 (3) Å, respectively. The Fe-OAr bond lengths in II and III are found at 2.057 (9) and 1.996 (9) Å, respectively. The electronic and ^1H NMR spectra and solution magnetic studies are reported. Zero field Mössbauer spectra of I, II, and III show one doublet that consists of two poorly resolved quadrupole doublets with very similar isomer shift values. A fitting procedure using two Lorentzian lines with the restriction of equal areas yields (at 77 K) δ_1 = 0.46, ΔE_{Q1} = 0.64, δ_2 = 0.48, and ΔE_{Q2} = 0.96 mm/s for I, δ_1 = 0.49, ΔE_{Q1} = 0.78, δ_2 = 0.50, and ΔE_{Q2} = 1.09 mm/s for II, and δ_1 = 0.48, ΔE_{Q1} = 0.91, δ_2 = 0.47, and ΔE_{Q2} = 1.19 mm/s for III. Cyclic voltammetric studies in CH_3CN and DMF show that I and III reduce reversibly by one electron while II shows quasi-reversible reduction.

Introduction

The redox-active, non-heme iron proteins (NHIP) ubiquitous in virtually all forms of life[2] contain inorganic Fe-S centers in a variety of structures. Crystallographic studies on numerous NHIP, from various sources,[3] have established this diversity in structure of such $Fe^{II}S_4$,[3] $Fe^{III}S_4$,[3] Fe_4S_4,[3,4] Fe_2S_2,[5] and Fe_3S_3.[6]

The synthesis of inorganic, active-site analogue complexes has been of paramount importance in understanding the fine electronic and structural details of these centers, which in a biological environment are anchored to the protein backbone via deprotonated cysteinyl residues. Detailed descriptions of the electronic and structural characteristics of such synthetic analogues as the $[Fe_4S_4(SR)_4]^{2-}$,[7-9] $[Fe_4S_4(SR)_4]^{3-}$,[10] $[Fe_2S_2(SR)_4]^{2-}$,[11] $[Fe(SR)_4]^{2-}$,[12] $[Fe(SR_4)]^-$,[13] and $[Fe(o\text{-xylyldithiol})_2]^{-,2-}$[14] complexes are now available primarily due to elegant studies by Holm, Ibers, and co-workers.[15] Comparative studies of the electronic and

[†] University of Michigan.
[‡] Nuclear Research Center "Demokritos".

(1) Department of Chemistry, University of Iowa, Iowa City, IA.
(2) (a) Orme-Johnson, W. H. *Annu. Rev. Biochem.* **1973**, *42*, 159. (b) Lovenberg, W., Ed. "Iron-Sulfur Proteins"; Academic Press: New York, 1977, Vol. III. (c) Averill, B. A.; Orme-Johnson, W. H. In "Metal Ions in Biological Systems"; Sigel, H., Ed.; Marcel Dekker: New York, **1978**; Vol. VII.
(3) (a) Watenpaugh, K. D.; Sieker, L. C.; Herriott, J. R.; Jensen, L. H. *Acta Crystalalogr., Sect. B* **1973**, *B29*, 943. (b) Jensen, L. H. In "Iron-Sulfur Proteins"; Lovenberg, W., Ed.; Academic Press: New York, 1973; Vol. II, Chapter 4. (c) Eklund, H.; Nordström, B.; Zeppezauer, E.; Soderlund, G.; Ohlesson, I.; Boiwe, T.; Bränden, C. I. *FEBS Lett.* **1974**, *44*, 200. (d) Eklund, H.; Nordström, B.; Zeppezaier, E.; Soderlund, G.; Ohlesson, I.; Boiwe, T.; Soderberg, B. O.; Tapia, O.; Bränden, C. I. *J. Mol. Biol.* **1976**, *102*, 27. (e) Adman, A. T.; Sieker, L. C.; Jensen, L. H. *J. Biol. Chem.* **1973**, *248*, 2987.
(4) Freer, S. T.; Alden, R. A.; Carter, C. W.; Kraut, J. *J. Biol. Chem.* **1975**, *250*, 46.
(5) Fakuyama, K.; Hase, T.; Matsumoto, S.; Tsukihara, T.; Katsube, Y.; Tanaka, N.; Kakudo, M.; Wada, K.; Matsubara, H. *Nature (London)* **1980**, *286*, 522.

0002-7863/84/1506-4500$01.50/0

structural properties between the Fe–S centers in the analogue complexes and the corresponding centers in most of the NHIP have established the credibility of the model complexes as nearly exact active-site analogues. Among the multitude of the known Fe–S proteins, there exist a small number of such proteins that exhibit somewhat unusual electronic properties. These properties, which are apparent mainly in the ^{57}Fe Mössbauer and EPR spectra, are not present in any of the available model complexes. In the ferredoxin from Bacillus stearothermophilus the ^{57}Fe Mössbauer spectrum of the $[Fe_4S_4]^{2+}$ center shows[16] a broadened, asymmetric, quadrupole doublet that can be attributed to the overlapping of at least two components and suggests that the iron atoms in the $[Fe_4S_4]^{2+}$ center are not precisely equivalent. The appearance of two resolved quadrupole doublets in the spectrum of the reduced form of the protein $[Fe_4S_4]^{+}$ shows that the reduction is localized predominantly on one pair of iron ions which become ferrous in character with the other pair remaining essentially unchanged. A two-component Mössbauer spectrum also is observed for the Fe–S center (P centers) in the Fe–Mo protein of nitrogenase and suggests the presence of inequivalent iron sites within the core.[17] As suggested previously,[18] such inequivalencies of the iron ions within the Fe_4S_4 cores may well be attributed to protein-imposed differences in the coordination environments of the Fe atoms.

Until recently Fe–S clusters containing the Fe_4S_4 unit in a mixed terminal ligand environment had not been isolated, although their presence had been detected in solution by ^{1}H NMR spectroscopic studies.[8,19,33] The synthesis, isolation, and structural characterization[20] of the first mixed terminal ligand "cubane" cluster $[Fe_4S_4(SPh)_2Cl_2]^{2-}$ has made available a prototype for the examination of the iron atoms in two different environments within the *same* Fe_4S_4 core. The same molecule has been a convenient starting material for the synthesis of the $[Fe_4S_4(X)_2(Et_2NCS_2)_2]^{2-}$ (X = SPh) clusters that contain both four- and five-coordinate iron atoms in the same core.[21]

In this paper we report in detail on the synthesis of the $[Fe_4S_4(SPh)_2Cl_2]^{2-}$, $[Fe_4S_4(OPh)_2Cl_2]^{2-}$, and $[Fe_4S_4(SPh)_2(p\text{-}CH_3PhO)_2]^{2-}$ clusters and on the molecular structures and properties of the Ph_4P^+ salts of these anions.

Experimental Section

Synthesis. The chemicals in this research were used as purchased. Dimethylformamide (DMF) was stored over 4A Linde molecular sieves for 24 h and then distilled under reduced pressure at ~30 °C. Acetonitrile (CH_3CN) was distilled from calcium hydride (CaH_2) before use. Commercial grade methylene chloride (CH_2Cl_2) was distilled from CaH_2. Absolute ethanol and diethyl ether were used without any further purification. Potassium phenyl mercaptide (KSPh) was obtained by the reaction of potassium metal with thiophenol in tetrahydrofuran under dinitrogen. With the exception of dibenzyl trisulfide (BzSSSBz) and KSPh all syntheses were carried out under a dinitrogen atmosphere in a Vacuum Atmospheres Dri-Lab glovebox. Elemental analyses, on samples dried under vacuum for 12 h, were performed by Galbraith Analytical Laboratories, Knoxville, TN.

Physical Methods. Visible and ultraviolet spectra were obtained on Cary Model 118 and 219 spectrophotometers. Proton NMR spectra were obtained on a JEOL FX90Q Pulse FT NMR spectrometer with Me_4Si as internal standard. Chemical shifts are reported in parts per million (ppm). The following convention is used whenever isotropically shifted NMR spectra are reported. A negative sign is assigned to a resonance appearing upfield from Me_4Si. A positive sign is given to absorptions occurring downfield from Me_4Si.

Electrochemical measurements were performed with a PAR Model 173 potentiostat/galvanostat and a PAR Model 175 universal programmer. The electrochemical cell used had platinum working and auxiliary electrodes. As reference electrode a saturated calomel electrode was used. All solvents used in the electrochemical measurements were properly dried and distilled, and tetra-*n*-butylammonium perchlorate (Bu_4NClO_4) was used as the supporting electrolyte. Normal concentrations used were ~0.001 M electroanalyte and 0.1 M in supporting electrolyte. Purified argon was used to purge the solutions prior to the electrochemical measurements. The powder diffraction diagrams were obtained by using a 114-mm diameter Debye–Scherrer type camera with Ni-filtered Cu Kα radiation (λ = 1.5418 Å).

Mössbauer spectra were measured from 4.2 K to room temperature with a constant acceleration spectrometer. The source was 100 mCi of ^{57}Co in Rh matrix and was held at room temperature.

Preparation of Compounds. Bis(tetraphenylphosphonium) Bis(thiophenolato)dichlorotetrakis(μ_3-sulfido)tetraferrate(2II,2III), $(Ph_4P)_2[Fe_4S_4(SPh)_2Cl_2]$ (I). The synthesis of this compound from the $[Fe_4(SPh)_6Cl_4]^{2-}$ "adamantane" and dibenzyl trisulfide has been published.[20] An alternative procedure for the synthesis of this cluster from $[Fe_2S_2(SPh)_4]^{2-}$ is as follows.

In a solution of 0.3 g (0.23 mmol) of $(Ph_4P)_2[Fe_2S_2(SPh)_4]$ in 30 mL of DMF was suspended 0.06 g (0.46 mmol) of anhydrous $FeCl_2$. The resulting heterogeneous mixture was stirred for 20 min, and the solution changed from purple to brown. Following filtration, 150 mL of diethyl ether was slowly added to the filtrate. Upon standing for ca. 2 h, 0.2 g of pure black crystals of $(Ph_4P)_2[Fe_4S_4(SPh)_2Cl_2]$ was deposited, isolated, and dried in vacuo; yield 66%. The X-ray powder pattern, visible spectra, and isotropically shifted NMR spectra of this compound are identical with those of an "authentic" sample prepared as described previously.[20]

Bis(tetraphenylphosphonium) Bis(phenolato)bis(thiophenolato)tetrakis(μ_3-sulfido)tetraferrate(2II,2III), $(Ph_4P)_2[Fe_4S_4(OPh)_2(SPh)_2]$ (IV). To a solution of 1.00 g (0.76 mmol) of $(Ph_4P)_2[Fe_4S_4(SPh)_2Cl_2]$ in 50 mL of CH_3CN was added 2.8 mL of an ethanolic KOPh, 8.4% solution (1.53 mmol), dropwise with stirring over 10 min. A slight change from brown to yellow brown was observed. The solution was filtered to remove the KCl byproduct, and to the filtrate ether was added to incipient crystallization. Upon standing overnight, dark microcrystals formed that were isolated and dried in vacuo. The amount of the product (1.0 g) represents a 92% yield.

Anal. Calcd for $Fe_4S_6O_2P_2C_{72}H_{60}$ (M_r = 1434): C, 60.25; H, 4.18; Fe, 15.62; S, 13.40; P, 4.32. Found: C, 59.10; H, 4.29; Fe, 15.94; S, 12.93; P, 4.46.

The compound is X-ray isomorphous to $(Ph_4P)_2Fe_4S_4(SPh)_4$ and shows a major electronic absorption at 428 nm.

Bis(tetraphenylphosphonium) Bis(phenolato)dichlorotetrakis(μ_3-sulfido)tetraferrate(2II,2III), $(Ph_4P)_2[Fe_4S_4(OPh)_2Cl_2]$ (II). To a solution of 1.00 g (0.86 mmol) of $(Ph_4P)_2[Fe_4S_4Cl_4]$[20,22] in 50 mL of dimethylformamide (DMF) was added 0.20 g (1.72 mmol) of solid NaOPh. After being stirred for 20 min, the brown-green solution was filtered and to the filtrate was added 200 mL of anhydrous ether. The oil that formed was crystallized from CH_3CN following the addition of anhydrous ether. A 0.95-g sample of analytically pure crystals was obtained; yield 86%. The compound is X-ray isomorphous to the $(Ph_4P)_2[Fe_4S_4(SPh)_2Cl_2]$.

Anal. Calcd for $Fe_4S_4Cl_2P_2O_2C_{60}H_{50}$ (M_r = 1287): C, 55.94; H, 3.88; Fe, 17.46; S, 9.94; Cl, 5.52. Found: C, 54.14; H, 3.96; Fe, 16.93; S, 10.36; Cl, 6.26.

(6) Stout, D. C.; Ghosh, D.; Pattabhi, V.; Robbins, A. H. *J. Biol. Chem.* **1980**, *255*, 1797.
(7) Averill, B. A.; Herskovitz, T.; Holm, R. H.; Ibers, J. A. *J. Am. Chem. Soc.* **1973**, *95*, 3523.
(8) Que, L.; Bobrik, M. A.; Ibers, J. A.; Holm, R. H. *J. Am. Chem. Soc.* **1974**, *96*, 4168.
(9) (a) Carrell, H. L.; Glusker, J. P.; Job, R.; Bruice, T. C. *J. Am. Chem. Soc.* **1977**, *99*, 3683. (b) Christou, G.; Garner, C. D.; Drew, M. G. B.; Cammack, R. *J. Chem. Soc., Dalton Trans.* **1981**, 1550.
(10) (a) Laskowski, E. J.; Frankel, R. B.; Gillum, W. O.; Papaefthymiou, G. C.; Renaud, J.; Ibers, J. A.; Holm, R. H. *J. Am. Chem. Soc.* **1978**, *100*, 5322. (b) Berg, J. J.; Hodgson, K. O.; Holm, R. H. *Ibid.* **1979**, *101*, 4586.
(11) Mayerle, J. J.; Denmark, S. E.; De Pamphilis, B. V.; Ibers, J. A.; Holm, R. H. *J. Am. Chem. Soc.* **1975**, *97*, 1032.
(12) Coucouvanis, D.; Swenson, D.; Baenziger, N. C.; Murphy, C.; Holah, D. G.; Sfarnas, N.; Simopoulos, A.; Kostikas, A. *J. Am. Chem. Soc.* **1981**, *103*, 3350.
(13) Millar, M.; Lee, J.; Koch, S. A.; Fikar, R. *Inorg. Chem.* **1982**, *21*, 4105.
(14) Lane, R. W.; Ibers, J. A.; Frankel, R. B.; Papaefthymiou, G. C.; Holm, R. H. *J. Am. Chem. Soc.* **1977**, *99*, 84.
(15) (a) Holm, R. H.; Ibers, J. A. In "Iron Sulfur Proteins"; Lovenberg, W., Ed.; Academic Press: New York, 1977; Chapter 7. (b) Holm, R. H. *Acc. Chem. Res.* **1977**, *10*, 427.
(16) Mullinger, R. N.; Cammack, R.; Rao, K. K.; Hall, D. O.; Dickson, D. P. E.; Johnson, C. E.; Rush, J. D.; Simopoulos, A. *Biochemistry* **1975**, *151*, 75.
(17) Münck, E.; Rhodes, H.; Orme-Johnson, W. H.; Davis, L. C.; Brill, W. J.; Shah, V. K. *Biochim. Biophys. Acta* **1975**, *400*, 32.
(18) Zimmerman, R.; Münck, E.; Brill, W. J.; Shah, V. K.; Henzl, M. T.; Rawlings, J.; Orme-Johnson, W. H. *Biochim. Biophys. Acta* **1978**, *537*, 185.
(19) Johnson, R. W.; Holm, R. H. *J. Am. Chem. Soc.* **1978**, *100*, 5338.
(20) Coucouvanis, D.; Kanatzidis, M.; Simhon, E.; Baenziger, N. C. *J. Am. Chem. Soc.* **1982**, *104*, 1874.
(21) Kanatzidis, M. G.; Ryan, M.; Coucouvanis, D.; Simopoulos, A.; Kostikas, A. *Inorg. Chem.* **1983**, *22*, 179.
(22) Bobrik, M. A.; Hodgson, K. O.; Holm, R. H. *Inorg. Chem.* **1977**, *16*, 1851.

Table I. Summary of Crystal Data, Intensity Collection, and Structure Solution and Refinement

	$(Ph_4P)_2[Fe_4S_4(SPh)_2Cl_2]$	$(Ph_4P)_2[Fe_4S_4(OPh)_2Cl_2]$	$(Ph_4P)_2[Fe_4S_4(SPh)_2(OC_6H_4CH_3)_2]$
formula	$Fe_4S_6Cl_2C_{60}H_{50}P_2$	$Fe_4S_4O_2Cl_2C_{60}H_{50}P_2$	$Fe_4S_6O_2C_{74}H_{64}P_2$
a, Å	13.082 (1)	13.060 (3)	24.595 (7)
b, Å	21.182 (4)	20.891 (5)	12.588 (3)
c, Å	21.376 (4)	21.423 (7)	10.877 (3)
V, Å^3	5923.34	5844.70	3367.53
Z	4	4	2
d_{calcd}, g/cm^3	1.48	1.46	1.45
d_{obsd},[a] g/cm^3	1.49	1.46	1.43
space group	*Pbcn*	*Pbcn*	$P2_12_12$
cryst dimens, mm	0.51 × 0.23 × 0.10	0.43 × 0.27 × 0.24	0.5 × 0.27 × 0.09
radiatn	Mo, λ(Kα) = 0.710 69 Å	Mo, λ(Kα) = 0.710 69 Å	Mo, λ(Kα) = 0.710 69 Å
abs. coeff μ, cm^{-1}	13.7	13.2	11.4
data collected	2θ = 40, $\pm h,\pm k,\pm l$	2θ = 40, $h,\pm k,\pm l$	2θ = 45, $\pm h,+k,\pm l$
unique data	2796	2756	3948
data used in refinement, $F_o^2 > 3\sigma(F_o^2)$	2203	2149	3231
no. of atoms in asymmetric unit	62	62	76
no. of variables	334	334	397
error in observn of unit weight	1.70	2.98	1.77
phasing technique	direct methods	direct methods	heavy atom
R,[b] %	6.2	6.1	6.58
R_w, %	8.2	8.2	8.45

[a] Determined by flotation in a CCl_4–pentane mixture. [b] $R = \sum||\Delta F|/\sum|F_o|$. [c] $R_w = [\sum w(\Delta F)^2/\sum w|F_o|^2]^{1/2}$.

Bis(tetraphenylphosphonium) Bis(thiophenolato)bis(*p*-methylphenolato)tetrakis(μ_3-sulfido)tetraferrate(2II,2III), $(Ph_4P)_2[Fe_4S_4(SPh)_2(p\text{-}MePhO)_2]$ (III). To a solution of 1.00 g (0.76 mmol) of $(Ph_4P)_2[Fe_4S_4(SPh)_2Cl_2]$ in 50 mL of CH_3CN was added 0.20 g (1.54 mmol) of solid Na-*p*-MePhO with stirring. After 2 h of stirring, the solution was filtered and to the brown filtrate was added anhydrous ether to incipient crystallization. Upon standing for 24 h, 0.5 g of black crystals was obtained in analytically pure form; yield 45%. This compound is X-ray isomorphous to the $(Ph_4P)_2[Fe_4S_4(SPh)_4]$.

Anal. Calcd for $Fe_4S_6O_2P_2C_{74}H_{64}$ (M_r = 1458): C, 60.74; H, 4.38; Fe, 15.32; S, 13.13. Found: C, 59.45; H, 4.58; Fe, 15.52; S, 13.95.

X-ray Diffraction Measurements. Collection of Data. Single crystals for I, II, III, and IV were obtained by the slow diffusion of diethyl ether into CH_3CN solutions of the complexes. These were sealed in quartz capillaries and used for data collection. Details concerning crystal characteristics and X-ray diffraction methodology are shown in Table I. For the $(Ph_4P)_2[Fe_4S_4(SPh)_2Cl_2]$ (I) crystal intensity data were obtained on a Picker-Nuclear four-circle diffractometer according to a protocol already described.[19] Intensity data for the Ph_4P^+ salts of $[Fe_4S_4(OPh)_2Cl_2]^{2-}$ (II) and $[Fe_4S_4(SPh)_2(p\text{-}MePhO)_2]^{2-}$, III were obtained on a Nicolet P3/F four-circle diffractometer. A detailed description of the instrument and the data acquisition procedures have been described previously.[23]

$(Ph_4P)_2[Fe_4S_4(XPh)_2Cl_2]$ [I, X = S; II, X = O]. The space group for the X-ray isomorphous I and II was determined by precession photographs of single crystals and was found to be *Pbcn*. The cell dimensions for I and II (Table I) were refined by using 24 well-centered reflections with 2θ values between 25° and 35° (Mo $K\alpha_1$, λ = 0.709 26 Å).

$(Ph_4P)_2[Fe_4S_4(SPh)_2(L)_2]$ (III, L = *p*-$CH_3C_6H_4O$; IV, C_6H_5O). The space group for these X-ray isomorphous complexes was found to be $P2_12_12$. The cell dimensions for III and IV were refined as described for I and II above.

Reduction of Data. The raw data were reduced to net intensities, estimated standard deviations were calculated on the basis of counting statistics, Lorentz-polarization corrections were applied, and equivalent reflections were averaged. The estimated standard deviation of the structure factor was taken as the larger of that derived from counting statistics and that derived from the scatter of multiple measurements.

The least-squares program used minimizes $\sum w(\Delta|F|)^2$. The weighting function used throughout the refinement of the structure gives zero weight to those reflections with $F^2 \leq 3\sigma(F^2)$ and $w = 1/\sigma^2(F)$ to all others $[\sigma^2(F^2) = (0.06F^2)^2 + \sigma^2(F^2)$ (from counting statistics)].[24]

The scattering factors of the neutral non-hydrogen atoms were taken from the tables of Doyle and Turner,[25] and real and imaginary dispersion corrections[26] were applied to all of them. The spherical hydrogen scattering factors tables of Stewart, Davidson, and Simpson[27] were used. Absorption corrections were applied by using the analytical program ABSORB[28] that uses the analytical method of de Meulenaer and Tompa.[29]

Determination of Structures. $(Ph_4P)_2[Fe_4S_4(XPh)_2Cl_2]$ (I, X = S; II, X = O). The structure of I was determined initially by using a limited data set ($2\theta_{max}$ = 30°, Mo $K\alpha_1$). A three-dimensional Patterson synthesis map was used to verify the correctness of the atomic positions of the two iron, three sulfur, and one chlorine atoms obtained by direct methods using the program MULTAN.[30] The $[Fe_4S_4(SPh)_2Cl_2]^{2-}$ anion is required by symmetry to reside on a crystallographic twofold axis. The remaining non-hydrogen atoms were located by subsequent Fourier syntheses following least-squares refinement of the input atomic coordinates. The refinement of all atoms in the asymmetric unit using isotropic temperature factors and the limited data set gave an R value of 0.10. Further refinement using higher order data (to 40°) with anisotropic temperature factors for the non-hydrogen atoms resulted in an R value of 0.071. At this stage an absorption correction was applied to the data and the hydrogen atoms were introduced at their calculated positions (C–H = 0.95 Å). In the final refinement the hydrogen atoms were included in the structure factor calculation but were not refined. The final R value was 0.062 and the weighted R_w was 0.082. During the last cycle of refinement all parameter shifts were less than 10% of their esd.

The structure of II was refined on data obtained over a half sphere of the reciprocal lattice ($2\theta_{max}$ = 40°). No absorption corrections were applied to the data. The atomic coordinates of the non-hydrogen atoms from the structure of I were used, and the thiophenolate sulfur atom was replaced by oxygen. After six cycles of refinement the hydrogen atom coordinates were calculated and the hydrogen atoms were input in the structure factor calculations but were not refined. In the cycle of refinement reported here, using anisotropic temperature factors for all non-hydrogen atoms, the R values are 0.061 and (weighted) 0.082. The positional parameter shifts at this stage average less than 0.2 esd for Fe, S, and Cl atoms and less than 0.3 esd for the atoms in the Ph_4P^+ cation but 1.9 esd for the atoms in the phenoxy group. Continued refinement gave lower R values but unreasonable values for the anisotropic temperature factors of the phenoxy group atoms.

$(Ph_4P)_2[Fe_4S_4(SPh)_2(L)_2]$ (III, L = *p*-$CH_3C_6H_4O^-$; IV, L = $C_6H_5O^-$). The structure of IV (L = $C_6H_5O^-$) was determined by using a data set obtained over half of the reflection sphere to a $2\theta_{max}$ of 45° (Mo $K\alpha_1$). A Patterson synthesis map revealed the positions of the two Fe atoms located near the crystallographic twofold axis at 0, $^1/_2$, z. Subsequent electron density Fourier maps were used to locate the remaining non-hydrogen atoms in the asymmetric unit. Refinement of all atoms with isotropic temperature factors converged to a conventional R value of 0.12.

(23) Kanatzidis, M. G.; Coucouvanis, D. *Inorg. Chem.* **1984**, *23*, 403.
(24) Grant, D. F.; Killean, R. C. G.; Lawrence, J. L. *Acta Crystallogr., Sect. B* **1969**, *B25*, 374.
(25) Doyle, P. A.; Turner, P. S. *Acta Crystallogr., Sect. A* **1968**, *A24*, 390.
(26) Cromer, D. T.; Liberman, D. *J. Chem. Phys.* **1970**, *53*, 1891.
(27) Stewart, R. F.; Davidson, E. R.; Simpson, W. T. *J. Chem. Phys.* **1965**, *42*, 3175.
(28) Templeton, L.; Templeton, D. "ABSORB"; American Crystallographers Association Meeting: Storrs, CT, Abstract E10, p 143; modified for local use by F. J. Hollander.
(29) deMeulenaer, J.; Tompa, H. *Acta Crystallogr.* **1965**, *19*, 1014.
(30) Main, P.; Woolfson, M. M.; Germain, G. "MULTAN A Computer Program for the Automatic Solution of Crystal Structures"; University of York: York, England, 1971.

Table II. Positional and Thermal Parameters[a] and Standard Deviations[b] for the Anion in $(Ph_4P)_2[Fe_4S_4(SPh)_2Cl_2]$

atom	*x*	*y*	*z*	atom	*x*	*y*	*z*
Fe(1)	0.0515 (1)	0.59713 (7)	0.30612 (6)	$CS_t(1)$	0.1733 (8)	0.7210 (6)	0.3617 (6)
Fe(2)	−0.0929 (1)	0.50705 (7)	0.28103 (7)	$CS_t(2)$	0.2490 (8)	0.7521 (7)	0.3956 (7)
S(1)	−0.0644 (2)	0.4910 (1)	0.1772 (1)	$CS_t(3)$	0.2792 (9)	0.8127 (7)	0.3773 (9)
S(2)	0.1188 (2)	0.6139 (1)	0.2101 (1)	$CS_t(4)$	0.237 (1)	0.8421 (7)	0.3269 (9)
$S_t(1)$	0.1323 (2)	0.6448 (2)	0.3868 (1)	$CS_t(5)$	0.162 (1)	0.8115 (7)	0.2935 (7)
Cl	−0.2218 (2)	0.4528 (2)	0.3207 (2)	$CS_t(6)$	0.132 (1)	0.7533 (7)	0.3093 (7)

atom	*B*(11)	*B*(22)	*B*(33)	*B*(12)	*B*(13)	*B*(23)
Fe(1)	2.58 (6)	4.40 (8)	4.35 (8)	−0.08 (6)	−0.10 (5)	−0.49 (6)
Fe(2)	2.29 (6)	4.42 (8)	5.70 (9)	−0.15 (5)	−0.24 (5)	1.24 (6)
S(1)	3.9 (1)	5.5 (2)	5.2 (2)	−0.1 (1)	−1.6 (1)	−1.4 (1)
S(2)	3.2 (1)	5.3 (1)	5.1 (1)	−1.2 (1)	0.81 (9)	−0.3 (1)
$S_t(1)$	5.2 (1)	7.0 (2)	5.8 (2)	−0.8 (1)	−1.3 (1)	−1.2 (1)
Cl	4.2 (1)	7.4 (2)	11.2 (2)	−0.8 (1)	1.7 (1)	3.2 (2)
$CS_t(1)$	3.6 (5)	6.4 (7)	7.3 (8)	0.2 (5)	−0.2 (5)	−1.6 (6)
$CS_t(2)$	4.0 (6)	6.6 (8)	10.2 (9)	0.3 (6)	−1.8 (6)	−3.3 (7)
$CS_t(3)$	3.7 (6)	4.4 (8)	15.2 (13)	−0.5 (6)	−0.9 (7)	−3.3 (8)
$CS_t(4)$	6.2 (8)	6.3 (9)	12.7 (13)	1.5 (8)	2.8 (8)	−2.3 (9)
$CS_t(5)$	5.8 (7)	5.5 (8)	9.7 (9)	0.2 (6)	0.7 (6)	−2.1 (7)
$CS_t(6)$	6.2 (7)	5.5 (8)	8.0 (9)	−0.2 (6)	0.9 (6)	−2.8 (6)

[a] The thermal parameters are in units of Å^2. The temperature factor has the form $T = -\sum(^1/_4\, B(IJ)H(I)H(J)\mathrm{ASTAR}(I)\mathrm{ASTAR}(J))$. *H* is the Miller index, ASTAR is the reciprocal cell length, and *I* and *J* are cycled 1 through 3. [b] Calculated standard deviations are indicated in parentheses.

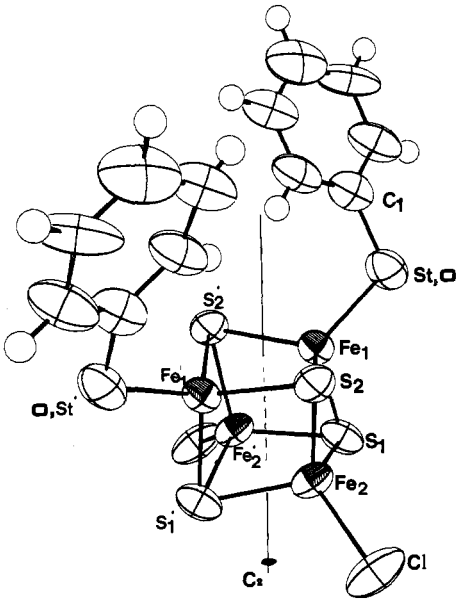

Figure 1. Structure and labeling of the $[Fe_4S_4(XC_6H_5)_2Cl_2]^{2-}$ anions (X = S, O). Thermal ellipsoids as drawn by ORTEP (Johnson, C. K. ORNL-3794; Oak Ridge National Laboratory: Oak Ridge, TN, 1965) represent the 50% probability surfaces for the anion with X = S.

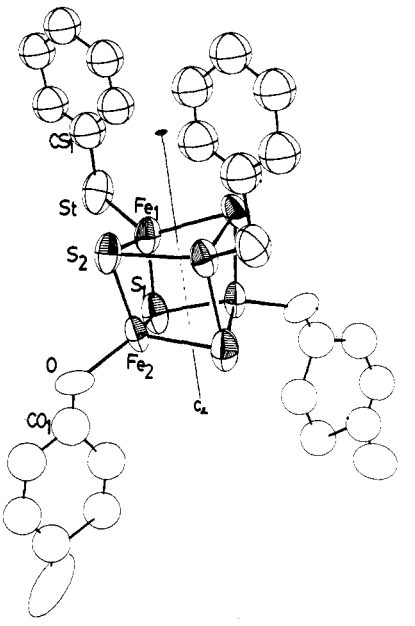

Figure 2. Structure and labeling of the $[Fe_4S_4(SC_6H_5)_2(OC_6H_4\text{-}p\text{-}CH_3)]^{2-}$ anion. Thermal ellipsoids as drawn by ORTEP represent the 50% probability surfaces.

In this refinement the positions of the oxygen and sulfur atoms were each given half occupancy of O and S to account for an apparent orientational disorder. In view of this disorder no further calculations were carried out. In an attempt to resolve the orientation disorder problem, a data set was obtained (full sphere, $2\theta_{max} = 45°$, Mo $K\alpha_1$) for the X-ray isomorphous $p\text{-}CH_3C_6H_4O^-$ derivative **III**. The coordinates obtained previously for IV were refined, and a difference Fourier electron density map was calculated. In this map the *p*-methyl carbon was located. The single site occupancy of this carbon and the temperature factor of the O and S atoms indicated that the anion was "locked" in a specific orientation with no evidence for disorder. With all atoms included, a least-squares calculation with isotropic temperature factors converged to an *R* value of 0.11. Anisotropic temperature factors were assigned to all non-hydrogen atoms and refinement converged to $R_w = 0.096$ and $R = 0.071$. At this stage the hydrogen atoms were included in the structure factor calculation at their calculated positions but were not refined (C–H = 0.95 Å). A final cycle of least-squares refinement resulted in values of $R_w = 0.084$ and $R = 0.066$. During the refinement the $\pm h,\pm k,\pm l$ data were not averaged to determine the "handedness" of the structure. Refinement of the enantiomorph converged to *R* values higher by ca. 1%.

Crystallographic Results. The final atomic positional and thermal parameters for the anions in $(Ph_4P)_2[Fe_4S_4(SPh)_2Cl_2]$, $(Ph_4P)_2[Fe_4S_4(OPh)_2Cl_2]$, and $(Ph_4P)_2[Fe_4S_4(p\text{-}CH_3PhO)_2(SPh)_2]$ with standard deviations derived from the inverse matrices of the least-squares refinements are compiled in Tables II, III, and IV, respectively. Intramolecular distances and angles forthe anions in all structures are given in Table V. The atom labeling schemes are shown in Figures 1 and 2. The atomic positional and thermal parameters for the Ph_4P^+ cations in all structures and stereoviews of crystal packing for I and II have been deposited as supplementary material.

The generated atomic parameters of the hydrogen atoms have been deposited together with tables of the observed values of *F*, their esd's, and the $|F_o| - |F_c|$ values. (See paragraph at the end of this paper regarding supplementary material.)

Results and Discussion

Syntheses and Characterization of the $[Fe_4S_4L_2L'_2]^{2-}$ Clusters. The synthesis of the mixed-ligand $[Fe_4S_4L_2Cl_2]^{2-}$ clusters is readily accomplished by stoichiometric reactions between $[Fe_4S_4Cl_4]^{2-}$ and PhS^- or PhO^- ligands. The $[Fe_4S_4(SPh)_2(OAr)_2]^{2-}$ clusters are obtained in a similar manner from $[Fe_4S_4(SPh)_2Cl_2]^{2-}$. The successful isolation of these clusters from equilibrium mixtures of $[Fe_4S_4(SPh)_nCl_{4-n}]^{2-}$ species is attributed mainly to the crystallization characteristics of the Ph_4P^+ salts that are relatively insoluble in the solvents employed. The use of dibenzyl trisulfide

Table III. Positional and Thermal Parameters[a] and Standard Deviations[b] for the Anion in $(Ph_4P)_2[Fe_4S_4(OPh)_2Cl_2]$

atom	x	y	z	atom	x	y	z
Fe(1)	0.0527 (1)	0.60504 (8)	0.30643 (8)	CO(1)	0.155 (2)	0.713 (1)	0.357 (1)
Fe(2)	−0.0924 (1)	0.51300 (7)	0.28219 (7)	CO(2)	0.240 (1)	0.743 (1)	0.3985 (9)
S(1)	0.0667 (2)	0.4975 (2)	0.3229 (1)	CO(3)	0.276 (1)	0.8120 (7)	0.3775 (9)
S(2)	−0.1175 (3)	0.6211 (1)	0.2918 (2)	CO(4)	0.237 (2)	0.839 (1)	0.332 (1)
Cl	0.2201 (2)	0.4578 (2)	0.1776 (2)	CO(5)	0.170 (2)	0.816 (1)	0.294 (1)
O	−0.1264 (7)	0.6505 (5)	0.1212 (5)	CO(6)	0.134 (1)	0.758 (1)	0.304 (1)

atom	B(11)	B(22)	B(33)	B(12)	B(13)	B(23)
Fe(1)	6.1 (1)	5.03 (9)	5.12 (9)	−0.77 (7)	0.70 (7)	−1.52 (7)
Fe(2)	3.71 (7)	4.47 (8)	4.88 (8)	0.09 (6)	0.28 (6)	0.86 (6)
S(1)	4.8 (2)	6.6 (2)	5.2 (2)	0.3 (1)	−0.8 (1)	1.3 (1)
S(2)	6.8 (2)	5.2 (2)	6.9 (2)	1.6 (1)	2.1 (1)	0.1 (1)
Cl	5.3 (2)	7.7 (2)	9.8 (2)	0.7 (2)	1.8 (2)	−3.0 (2)
O	8.7 (6)	5.0 (6)	19.6 (9)	2.5 (5)	3.0 (6)	8.7 (6)
CO(1)	9.7 (16)	14.6 (14)	9.9 (14)	4.5 (13)	−3.2 (12)	−6.0 (12)
CO(2)	10.7 (12)	19.1 (16)	15.6 (12)	8.3 (12)	1.1 (10)	−5.9 (12)
CO(3)	6.9 (8)	9.5 (7)	22.2 (14)	−4.5 (7)	4.8 (9)	−12.2 (9)
CO(4)	20.3 (21)	15.6 (20)	16.5 (20)	10.6 (18)	3.0 (15)	0.7 (15)
CO(5)	17.1 (19)	8.9 (15)	17.4 (20)	−1.2 (14)	6.7 (15)	−6.8 (14)
CO(6)	10.0 (11)	8.0 (10)	14.3 (15)	−1.6 (9)	0.9 (10)	−4.1 (10)

[a] See footnote *a*, Table II. [b] See footnote *b*, Table II.

Table IV. Positional and Thermal Parameters[a] and Standard Deviations[b] for the Anion in $(Ph_4P)_2[Fe_4S_4(SPh)_2(p\text{-}CH_3PhO)_2]$

atom	x	y	z	atom	x	y	z
Fe(1)	0.51527 (6)	0.3946 (1)	0.7295 (1)	CO(5)	0.6144 (6)	0.583 (1)	0.309 (1)
Fe(2)	0.55485 (6)	0.5308 (1)	0.9038 (1)	CO(6)	0.5996 (5)	0.5765 (8)	0.190 (1)
S(1)	0.4786 (1)	0.6336 (2)	0.9389 (3)	CO(7)	0.687 (1)	0.610 (2)	0.457 (2)
S(2)	0.5697 (1)	0.5362 (2)	0.6939 (3)	CS(1)	0.4672 (5)	0.7663 (9)	0.501 (1)
S_t	0.5333 (2)	0.2274 (2)	0.6572 (3)	CS(2)	0.4642 (6)	0.6755 (8)	0.431 (1)
O	0.6252 (3)	0.5802 (6)	0.9750 (7)	CS(3)	0.4671 (7)	0.682 (1)	0.306 (2)
CO(1)	0.6360 (5)	0.5857 (8)	0.084 (2)	CS(4)	0.4710 (6)	0.776 (1)	0.237 (2)
CO(2)	0.6874 (7)	0.0036 (9)	0.115 (1)	CS(5)	0.4717 (6)	0.863 (1)	0.299 (2)
CO(3)	0.7044 (5)	0.6097 (7)	0.235 (2)	CS(6)	0.4685 (5)	0.8672 (8)	0.429 (2)
CO(4)	0.6724 (8)	0.6023 (9)	0.335 (1)				

atom	B(11)	B(22)	B(33)	B(12)	B(13)	B(23)
Fe(1)	4.97 (9)	4.98 (7)	7.40 (8)	−0.54 (6)	−0.08 (7)	−0.20 (6)
Fe(2)	4.38 (8)	4.79 (7)	7.50 (8)	−1.02 (7)	0.28 (7)	−0.20 (6)
S(1)	5.8 (2)	5.3 (1)	8.1 (2)	−0.6 (1)	0.2 (1)	−0.9 (1)
S(2)	4.9 (1)	5.4 (1)	8.1 (1)	−0.7 (1)	1.1 (7)	0.1 (1)
S_t	8.0 (2)	4.9 (1)	10.2 (2)	−0.3 (1)	−1.5 (2)	0.3 (1)
O	5.4 (5)	5.5 (4)	4.8 (3)	−0.1 (3)	1.1 (3)	−0.3 (3)
CO(1)	1.6 (6)	2.8 (4)	18.7 (15)	−0.6 (4)	0.7 (9)	0.3 (7)
CO(2)	8.0 (10)	4.7 (6)	9.4 (8)	−0.4 (6)	−0.7 (7)	−0.3 (6)
CO(3)	6.6 (7)	2.4 (4)	12.8 (11)	−0.5 (4)	0.2 (8)	−0.4 (6)
CO(4)	13.1 (13)	4.5 (6)	5.1 (6)	0.8 (7)	−2.5 (8)	0.3 (5)
CO(5)	4.6 (7)	8.6 (8)	9.2 (8)	0.6 (6)	−1.5 (6)	−1.7 (7)
CO(6)	5.4 (7)	4.9 (5)	9.1 (8)	−1.2 (5)	−1.6 (6)	−1.8 (5)
CO(7)	16.8 (19)	10.1 (11)	15.4 (16)	4.8 (13)	1.0 (14)	3.6 (11)
CS(1)	4.3 (6)	5.2 (6)	9.8 (8)	0.5 (5)	1.0 (5)	0.8 (5)
CS(2)	8.3 (9)	3.1 (5)	8.9 (8)	1.5 (5)	1.6 (6)	0.3 (5)
CS(3)	9.6 (11)	6.6 (7)	12.4 (12)	2.2 (7)	1.6 (9)	−1.5 (8)
CS(4)	7.9 (10)	6.6 (7)	11.8 (10)	0.1 (7)	0.1 (8)	2.1 (8)
CS(5)	7.1 (9)	7.1 (8)	12.5 (11)	−2.1 (7)	−1.9 (8)	2.3 (9)
CS(6)	6.5 (8)	3.6 (5)	12.6 (10)	−0.5 (5)	−0.2 (7)	0.1 (6)

[a] See footnote *a*, Table II. [b] See footnote *b*, Table II.

as both an oxidizing agent and a source of S^{2-} in homogeneous solutions has been described previously.[31,32] A general synthetic scheme is shown in Figure 3.

The electronic spectra of the mixed-ligand clusters (Table VI) are essentially composite of the spectra reported for the identical ligand environment clusters. The latter have been described in detail.[15,33]

Crystallographic Studies. Description of the Structures of the $(Ph_4P)_2[Fe_4S_4(XPh)_2Cl_2]$ (I, X = S; II, X = O) Complexes. The crystal structures of the isomorphous and isostructural $(Ph_4P)_2$-

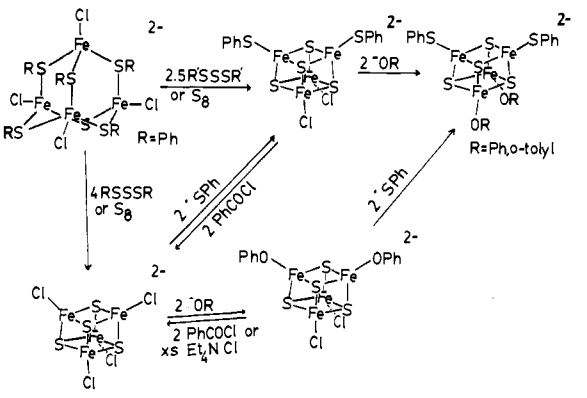

Figure 3. Synthesis and interconversions of the $[Fe_4S_4(L)_2(L')_2]^{2-}$ mixed-ligand cubane clusters.

(31) Coucouvanis, D.; Swenson, D.; Stremple, P.; Baenziger, N. C. *J. Am. Chem. Soc.* **1979**, *101*, 3392.

(32) Coucouvanis, D.; Stremple, P.; Simhon, E. D.; Swenson, D.; Baenziger, N. C.; Draganjac, M.; Chan, L. T.; Simopoulos, A.; Papaefthymiou, V.; Kostikas, A.; Petrouleas, V. *Inorg. Chem.* **1983**, *22*, 293.

(33) Cleland, W. E.; Holtman, D. A.; Sabat, M.; Ibers, J. A.; DeFotis, G. C.; Averill, B. A. *J. Am. Chem. Soc.* **1983**, *105*, 6021.

Table V. Selected Distances (Å) and Angles in the Anions[a] of the Ph_4P^+ Salts of $[Fe_4S_4^*(SPh)_2Cl_2]^{2-}$ (I), $[Fe_4S_4^*(OPh)_2Cl_2]^{2-}$ (II), and $[Fe_4S_4^*(SPh)_2(p\text{-}CH_3PhO)_2]^{2-}$ (III)

	I	II	III		I	II	III
	Distances				Angles		
Fe(1)–Fe(1)′	2.751 (3)	2.782 (4)	2.759 (3)	Fe(1)–S(2)–Fe(1)′	74.52 (9)	75.14 (12)	74.46 (10)
Fe(2)–Fe(2)′	2.770 (3)	2.780 (3)	2.808 (3)	Fe(2)–S(1)–Fe(2)′	75.08 (10)	74.81 (11)	75.82 (11)
Fe(1)–Fe(2)′	2.721 (2)	2.749 (2)	2.736 (2)	Fe(1)–S(1)′–Fe(2)′	73.30 (9)	73.84 (10)	73.54 (9)
Fe(1)–Fe(2)	2.738 (2)	2.752 (2)	2.730 (2)	Fe(1)–S(1)′–Fe(2)	73.96 (8)	74.19 (10)	72.45 (10)
mean[b]	2.745 (10)	2.766 (9)	2.758 (18)	Fe(2)–S(2)–Fe(1)′	73.45 (9)	73.75 (10)	72.61 (10)
Fe(1)–S(1)	2.282 (3)	2.281 (3)	2.310 (3)	Fe(2)–S(2)–Fe(1)	73.30 (9)	74.13 (10)	73.41 (9)
Fe(2)–S(2)	2.297 (3)	2.292 (3)	2.313 (3)	mean	73.9 (3)	74.3 (2)	73.7 (5)
Fe(1)–S(2)	2.262 (3)	2.293 (3)	2.263 (3)	Fe(2)–Fe(1)–Fe(2)′	60.98 (5)	60.71 (6)	61.82 (5)
Fe(1)–S(2)′	2.282 (3)	2.269 (4)	2.297 (3)	Fe(1)–Fe(2)–Fe(1)′	60.52 (5)	60.76 (6)	60.63 (5)
Fe(2)′–S(1)′	2.269 (3)	2.277 (3)	2.260 (3)	Fe(2)–Fe(1)–Fe(1)′	59.44 (5)	59.66 (6)	59.57 (5)
Fe(2)′–S(1)	2.277 (3)	2.299 (3)	2.309 (4)	Fe(2)′–Fe(1)–Fe(1)′	60.04 (5)	59.57 (6)	59.79 (5)
mean	2.278 (5)	2.285 (5)	2.292 (10)	mean	60.2 (3)	60.2 (3)	60.5 (5)
S(1)–S(1)′	3.540 (4)	3.577 (6)	3.523 (5)	S(1)–Fe(1)–S(2)	105.5 (1)	104.2 (2)	104.6 (1)
S(2)–S(2)′	3.546 (4)	3.554 (6)	3.547 (5)	S(1)–Fe(1)–S(2)′	104.4 (1)	104.9 (2)	106.5 (1)
S(1)–S(2)	3.618 (5)	3.591 (4)	3.690 (5)	S(2)–Fe(1)–S(2)′	102.6 (1)	102.3 (2)	102.1 (2)
S(1)–S(2)′	3.608 (4)	3.626 (4)	3.617 (5)	S(1)′–Fe(2)′–S(2)′	104.6 (2)	103.6 (2)	105.9 (1)
mean	3.578 (20)	3.587 (15)	3.59 (4)	S(1)′–Fe(2)′–S(1)	102.3 (1)	102.8 (2)	100.9 (2)
Fe(1)–S_t	2.261 (3)		2.289 (3)	S(1)–Fe(2)′–S(2)′	104.4 (1)	104.3 (2)	104.5 (1)
Fe–O_t		2.057 (9)	1.996 (9)	mean	104.0 (5)	103.6 (4)	104.0 (9)
Fe(2)–Cl	2.210 (3)	2.203 (3)		S_t–Fe(1)–S(1)	106.6 (1)	107.5 (4)	100.7 (2)
				S_t–Fe(1)–S(2)	116.1 (1)	116.8 (4)	117.8 (2)
				S_t–Fe(1)–S(2)′	120.2 (1)	119.6 (3)	123.5 (2)
				mean	114.3 (4.0)	114.6 (3.3)	114.0 (6.8)
				Cl–Fe(2)–S(1)′	115.0 (2)	114.8 (2)	
				Cl–Fe(2)–S(1)	117.5 (2)	117.8 (2)	
				Cl–Fe(2)–S(2)	111.6 (2)	111.8 (2)	
				mean	114.7 (1.7)	114.8 (1.7)	
				O–Fe(2)–S(1)			117.7 (2)
				O–Fe(2)–S(1)′			122.4 (3)
				O–Fe(2)–S(2)			103.7 (2)
				mean			114.6 (5.6)

[a] For the cation in I, $[(C_6H_5)_4P]_2[Fe_4S_4^*(SC_6H_5)_2Cl_2]$, the four P–C bonds are within the range of 1.786 (10)–1.816 (10) Å with a mean value of 1.799 (15) Å. The C–C bonds are within the range of 1.337 (13)–1.417 (13) Å with a mean value of 1.375 (20) Å. The six C_i–P–C_j angles are found between 105.6 (1) and 112.3 (1)° with a mean value of 109 (2)°. The C–C–C angles are in the range from 118.0 (1) to 122.2 (1)° with a mean value of 119 (2)°. For the cations scatter estimate has been obtained as follows: $s = [\sum_{i=1}^{N}(X_i - \bar{X})^2/N - 1]^{1/2}$, where X_i is the value of an individual bond or angle and X is the mean value for the N equivalent bond lengths or angles. Intermolecular H contacts shorter than 2.82 Å were not found. For the cation in III, $[(C_6H_5)_4P]_2[Fe_4S_4(SC_6H_5)_2(p\text{-}CH_3C_6H_4O)_2]$, the four P–C bonds are within the range of 1.784 (10)–1.810 (10) Å with a mean value of 1.798 (12) Å. The C–C bonds are in the range from 1.289 (15) to 1.414 (16) Å with a mean value of 1.366 (25) Å. The six C_i–P–C_j angles are found between 108.4 (1) and 110.8 (1)° with a mean value of 109 (1)°. The C–C–C angles range from 116.9 (1) to 122.3 (1)° with a mean value of 119 (2)°. Intermolecular H contacts shorter than 2.95 Å were not found. For the cation in II, $[(C_6H_5)_4P]_2[Fe_4S_4^*(OC_6H_5)_2Cl_2]$ the four P–C bonds are within the range from 1.780 (11) to 1.814 (11) Å with a mean value of 1.795 (14) Å. The C–C bonds are in the range from 1.30 (2) to 1.43 (2) Å with a mean value of 1.38 (3) Å. The six C_i–P–C_j angles are found between 105.8 (1) and 111.1 (1)° with a mean value of 109 (2)°. The C–C–C angles range from 122.7 (1.4) to 117.4 (1.4)° with a mean value of 12o (1.4)°. [b] The standard deviation from the mean, σ, is reported: $\sigma = [\sum_{i=1}^{N}(X_i - \bar{X})^2/N(N-1)]^{1/2}$.

Table VI. Electronic Spectra of $[Fe_4S_4(L)_2(L')_2]^{2-}$ Clusters

	λ, nm	ε, cm^{-1} M^{-1}
$(Ph_4P)_2[Fe_4S_4(SPh)_2Cl_2]$[a]	452, 670 (sh)	7200, 1583
$(Ph_4P)_2[Fe_4S_4(OPh)_2Cl_2]$[a]	668 (sh)	<1800
$(Ph_4P)_2[Fe_4S_4(SPh)_2(OPh)_2]$[a]	414	10860
$(Ph_4P)_2[Fe_4S_4(SPh)_2Br_2]$[a]	440, 660 (sh)	8290, 2360
$(Ph_4P)_2[Fe_4S_4(SPh)_2Cl_2]$[b]	454, 670 (sh)	8490, 2200
$(Ph_4P)_2[Fe_4S_4(OPh)_2Cl_2]$[b]	666 (sh)	<2000
$(Ph_4P)_2[Fe_4S_4(SPh)_2(OPh)_2]$[b]	420	7400
$(Ph_4P)_2[Fe_4S_4(SPh)_2Br_2]$[b]	452, 662 (sh)	10700, 3870

[a] In CH_3CN. [b] In DMF.

$[Fe_4S_4(XPh)_2Cl_2]$ (X = O, S) consist of discrete cations and anions. The cations have their expected unexceptional geometry. As in other structures[7-9,33] in this class of Fe–S clusters, the $Fe_4S_4^*$ cores in the anions have a distorted cubic geometry that can be defined in terms of two interpenetrating tetrahedra (Fe_4 and S_4^*). Each of the anions in I and II are located on a crystallographic twofold axis of symmetry that coincides with the twofold molecular axis in idealized point group symmetry C_{2v} (Figure 1). The average values of the S*–Fe–S* and Fe–S*–Fe angles in I at 104.0 (5)° and 73.9 (3)° and in II at 103.6 (4)° and 74.3 (2)° are quite similar to corresponding values in the structures of other clusters that contain the $[Fe_4S_4^*]^{2+}$ units and underscore the rhombic, nonplanar geometry of the eight $Fe_2S_2^*$ faces of the $Fe_4S_4^*$ polyhedron. An examination of the Fe_4 and S_4^* tetrahedra reveals that, individually, they undergo a D_{2d} type of distortion along the idealized $\bar{4}$ axis that is coincident with the crystallographic twofold axis. These distortions result in *compressed* Fe_4 tetrahedra and *elongated* S_4^* tetrahedra.

In virtually all of the identical terminal ligand clusters that contain the $[Fe_4S_4^*]^{2+}$ core and have been characterized structurally, the 12 Fe–S* bonds are divided metrically into two sets of four short and eight long distances, respectively. The consistent appearance of this distortion that is observed in the structures of the $[Fe_4S_4^*(L)_4]^{n-}$ clusters (Table VII) (L = $PhCH_2S^-$, n = 2;[7] L = PhS^-, n = 2;[8] L = Cl^-, n = 2;[22] L = $(SCH_2CH_2CO_2)^{2-}$, n = 6;[9] L = t-BuS^-, n = 2;[34] L = PhO^-, n = 2[33]) has led to the suggestion[35] that compression along the idealized $\bar{4}$ axis represents the intrinsically stable configuration of the $[Fe_4S_4^*]^{2+}$ cores in this oxidation level.

In the structures of I and II the distortion of the $[Fe_4S_4^*]^{2+}$ cores from idealized T_d symmetry divides the structural parameters

(34) Mascharak, P. K.; Hagen, K. S.; Spence, J. T.; Holm, R. H. *Inorg. Chim. Acta* **1983**, *80*, 157.
(35) Laskowski, E. J.; Reynolds, J. G.; Frankel, R. B.; Foner, S.; Papaefthymiou, G. C.; Holm, R. H. *J. Am. Chem. Soc.* **1979**, *101*, 6562.

Table VII. Comparison of the $[Fe_4S_4]^{2+}$ cores[a] in representative examples of the $[Fe_4S_4(L)_4]^{2-}$ and $[Fe_4S_4(L)_2(L')_2]^{2-}$ Complexes

dist	$[Fe_4S_4(SPh)_4]^{2-}$[b]	$[Fe_4S_4(SCH_2Ph)_4]^{2-}$[c]	$[Fe_4S_4Cl_4]^{2-}$[d]	$[Fe_4S_4(SPh)_2Cl_2]^{2-}$[e]	$[Fe_4S_4(OPh)_2Cl_2]^{2-}$[e]	$Fe_4S_4(SPh)_2(p\text{-}CH_3PhO)_2]^{2-}$[e]	$[Fe_4S_4(OPh)_4]^{2-}$[f]
Fe–Fe(6)[g]	*2.763 (3)*	*2.746 (10)*	*2.766 (5)*	*2.745 (10)*	*2.766 (9)*	*2.758 (18)*	*2.753 (13)*
Fe–Fe(2)[h]	2.730 (2)	2.776 (10)	2.755 (2)	2.760	2.781 (2)	2.784[i], 2.730[j]	2.739
Fe–Fe(4)[h]	2.738 (4)	2.732 (5)	2.771 (4)	2.729	2.752 (2)	2.733, 2.767 (21)	2.760 (3)
Fe–S(12)[g]	*2.286 (5)*	*2.286 (10)*	*2.283 (5)*	*2.278 (5)*	*2.285 (5)*	*2.293 (10)*	*2.294 (8)*
Fe–S(4)[h]	2.267 (5)	2.239 (4)	2.260 (4)	2.289	2.287	2.311, 2.262	2.259 (7)
Fe–S(8)[h]	2.296 (4)	2.310 (3)	2.295 (3)	2.272 (4)	2.284 (7)	2.82 (12), 2.307 (4)	2.312 (8)
S–S(6)[g]	*3.611 (13)*	*3.605 (13)*	*3.587 (16)*	*3.578 (20)*	*3.587 (15)*	*3.59 (4)*	*3.619 (25)*
S–S(2)[h]	3.650 (3)	3.645 (3)	3.637 (2)	3.543	3.564	3.54, 3.690	3.696
S–S(4)[h]	3.591 (6)	3.586 (4)	3.562 (6)	3.613	3.607	3.65, 3.56 (2)	3.580 (11)

[a] The mean values of chemically equivalent bonds are reported. The standard deviations in parentheses (when more than two independent distances are averaged) are the larger of the standard deviations for an individual value estimated from the inverse matrix or of the standard deviation $\sigma = [\sum_{i=1}^{N}(X_i - \bar{X})^2/N(N-1)]^{1/2}$. [b] Reference 8. [c] Reference 7. [d] Reference 22. [e] This work. [f] Reference 33. [g] The values in parentheses represent the number of bonds of this type in the molecule. [h] The values in parentheses represent the number of bonds in the sets that result when the Fe_4S_4 cores are distorted from idealized T_d—$\bar{4}3m$ symmetry toward D_{2d}—$\bar{4}2m$. The idealized $\bar{4}$ axis is coincident with the crystallographic twofold axis in the $[Fe_4S_4(L)_2(L')_2]^{2-}$ anions (Figures 2 and 3). [i] These sets represent distortions along the crystallographic twofold axis. [j] These sets represent distortions along an axis that passes through the midpoints of the Fe(1),S(1)′,Fe(2)′,S(2)′ and Fe(1)′,S(1),Fe(2),S(2) rhombic units.

into the sets: Fe–Fe (2 + 4), S*–S* (2 + 4), Fe–Fe–Fe (4 + 8), S*–S*–S* (4 + 8) (Table V). However, *the 12 Fe–S* bonds in I and II are not divided metrically into two sets of four short and eight long distances*, respectively, and the structures of the $[Fe_4S_4^*]^{2+}$ cores in I and II represent the first examples of such cores without an overall compressed D_{2d} geometry.

The mean values of the Fe–S* bond lengths in I and II at 2.278 (5) and 2.285 (5) Å, respectively, are quite similar to corresponding values in the $[Fe_4S_4L_4]^{2-}$ clusters structurally characterized previously (Table VII). It appears that the very similar Fe–S* bond lengths in all of the $[Fe_4S_4^*]^{2+}$ cores are maintained within a narrow range by appropriate adjustments (distortions) of the Fe_4 and S_4* tetrahedra.

Description of the Structure of the $(Ph_4P)_2[Fe_4S_4(SPh)_2(p\text{-}CH_3C_6H_4O)_2]$ (III) Complex. The anions in III are located on crystallographic twofold axes and are well separated from each other by Ph_4P^+ cations. The structures of the cations are unexceptional and will not be discussed any further. The Fe_4S_4* core in III shows (Figure 2) and the same basic structural characteristics (Table V) typical for this unit which already have been described for I and II as well as for a plethora of other structures.[7-9,22,33,34] An analysis of the fine structural details of the core shows that, along one of the idealized $\bar{4}$ axes of the Fe_4S_4* core the Fe–S* distances, can be divided metrically into two sets of eight long and four short bonds with mean values of 2.307 and 2.262 Å, respectively.

This axis that is perpendicular to the crystallographic twofold axis is the only direction along which a compression of the Fe_4S_4* unit is evident. Along this same axis the Fe_4 tetrahedron is marginally elongated while the S_4* tetrahedron is compressed (Tables V and VII). An attempt to separate the Fe–S* bonds into sets of four and eight relative to the idealized $\bar{4}$ axis coincident with the crystallographic twofold axis did not show a significant (within 3σ) distinction between the two sets. It appears therefore that the distortion of the Fe_4S_4* core in III, at least marginally, can be described as a compression along an idealized $\bar{4}$ axis perpendicular to the crystallographic twofold axis.

The terminal Fe–SPh bond lengths in III (Table V) at 2.289 (3) Å are somewhat longer than the corresponding bonds in I. The Fe–OAr bond lengths in II and III at 2.057 (9) and 1.996 (9) Å, respectively, are appreciably *and significantly* longer than the Fe–O bond in the $[Fe^{III}(OAr)_4]^-$ complexes[36] at 1.847 (13) Å (R = 2,3,5,6-Me_4C_6H) and 1.866 (6) Å (R = 2,4,6-$Cl_3C_6H_3$). This difference can be explained on the basis of the expected variation in ionic radii with iron oxidation state[37] and consistent with a formal +2.5 oxidation state for the iron atoms in II and III. The difference in the Fe–OPh bond lengths between either II or III and the $[Fe_4S_4(OPh)_4]^{2-}$ cluster[33] (Fe–O = 1.865 (17) Å) is difficult to explain in view of the very similar Mössbauer parameters (Table VIII, vide infra) and apparently the same formal Fe oxidation state in the three clusters.

Table VIII. Isomer Shifts[a] and Quadrupole Splittings of $[Fe_4S_4(L)_2(L')_2]^{2-}$

complex	T, K	δ_1, mm s^{-1}	ΔE_{Q_1}, mm s^{-1}	δ_2, mm s^{-1}	ΔE_{Q_2}, mm s^{-1}
$[Fe_4S_4(SPh)_4]^{2-}$	300	0.31 ± 0.01[b]	0.63 ± 0.01[b]		
	77	0.43	0.93		
	4.2	0.46	1.07		
$[Fe_4S_4Cl_4]^{2-}$	300	0.38	0.38		
	77	0.49	0.67		
	4.2	0.52	1.09		
$[Fe_4S_4(OPh)_4]^{2-}$[c]	4.2	0.50	1.21		
$[Fe_4S_4(OPh)_2Cl_2]^{2-}$	77	0.49	0.78	0.50	1.09
	4.2	0.51	1.01	0.52	1.28
$[Fe_4S_4(SPh)_2(OPH)_2]^{2-}$	300	0.38	0.62	0.36	0.79
	77	0.48	0.91	0.47	1.19
	4.2	0.47	0.96	0.46	1.24
$[Fe_4S_4(SPh)_2Cl_2]^{2-}$	300	0.37	0.39	0.36	0.60
	77	0.46	0.64	0.48	0.96
	4.2	0.48	0.90	0.51	1.22

[a] With respect to Fe metal at room temperature. [b] Estimated uncertainty from computer fitting. [c] Values taken from ref 33.

The Structures of the $[Fe_4S_4]^{2+}$ Cores. In the structures of the $[Fe_4S_4L_4]^{2-}$ cubanes with identical terminal ligands,[7-9,22,33,34] the approximate D_{2d} compressed geometry of the $[Fe_4S_4^*]^{2+}$ cores is a persistent feature. The origin of this systematic distortion at present is not easily understood and has been the subject of controversy. Early qualitative treatments[38] and subsequently a SCF Xα calculation[39] for the $[Fe_4S_4(SR)_4]^{2-}$ clusters assuming a "cube" model[40] of T_d symmetry, arrived at orbitally degenerate ground states (four electrons in the triply degenerate $8t_2$ orbital). Supported by these calculations, the persistent distortions apparent in the core structures of the $[Fe_4S_4L_4]^{2-}$ cubanes were rationalized in terms of the Jahn–Teller effect.[39] The distortions that occur along the idealized $\bar{4}$ axis (in a $[Fe_4S_4^*]^{2+}$ core of idealized T_d symmetry) could correspond to a Jahn–Teller active vibrational mode of E symmetry and would be expected if the $[Fe_4S_4L_4]^{2-}$ clusters were characterized by orbitally degenerate ground states.

More recent theoretical calculations[41] on the $[Fe_4S_4L_4]^{2-}$ clusters (L = H, CH_3) considering more realistic T_d or D_{2d} symmetries and choosing atomic sphere radii that result in sphere overlapping show the highest occupied molecular orbitals of different sym-

(36) Koch, S. A.; Millar, M. *J. Am. Chem. Soc.* **1982**, *104*, 5255.
(37) (a) Shannon, R. D.; Prewitt, C. T. *Acta Crystallogr., Sect. B* **1969**, *B25*, 925. (b) Shannon, R. D. *Acta Crystallogr., Sect. A* **1976**, *A32*, 751.
(38) (a) Fourst, A. S.; Dahl, L. F. *J. Am. Chem. Soc.* **1970**, *92*, 7337. (b) Gall, R. S.; Chu, C. T.; Dahl, L. F. *Ibid.* **1974**, *96*, 4019. (c) Trinh-Toan; Teo, B. J.; Ferguson, J. A.; Meyer, T. J. *Ibid.* **1977**, *99*, 408.
(39) Yang, C. Y.; Johnson, K. H.; Holm, R. H.; Norman, J. G., Jr. *J. Am. Chem. Soc.* **1975**, *97*, 6596.
(40) In this model the iron and sulfur atoms are assumed to occupy the corners of a cube. This assumption leads to equal Fe–Fe and S*–S* bond lengths and imposes 90° S*–Fe–S* and Fe–S*–Fe angles.
(41) Aizman, A.; Case, D. A. *J. Am. Chem. Soc.* **1982**, *104*, 3269.

metry. In T_d symmetry this later calculation shows the highest occupied molecular orbital of e symmetry completely filled with four electrons. In D_{2d} symmetry the highest occupied molecular orbital is of b symmetry. On this basis it was argued that the $[Fe_4S_4L_4]^{2-}$ cubanes would not be expected to show a static Jahn–Teller effect. A similar conclusion was reached when the calculations were carried out in an unrestricted manner with "broken symmetry" (C_{2v}) orbitals in a valence bond approach.[41] Arguments against the validity of the Jahn–Teller effect as the cause of the D_{2d} distortion also have been presented by Thompson[42] who indicated that even if the ground state was orbitally degenerate (a t_2^4 electronic configuration), it is not likely that a *diamagnetic* ground state (evident in low-temperature magnetic measurements) would arise by a Jahn–Teller distortion.

The solid-state structures of I and II provide with *the first examples of* $[Fe_4S_4^*]^{2+}$ *cores that do not show an overall compressed* D_{2d} *geometry.* It is difficult to ascertain whether the undistorted geometry of the cores in the X-ray isomorphous I and II is exceptional or it reflects solid-state constraints imposed by the lattice. It should be emphasized, however, that there are no indications of unusually close interionic contacts in the lattice and that the Mössbauer spectral parameters (vide infra) for I and II in the solid state and in solution are virtually identical.

An inherent geometric feature of I and II by comparison to other $[Fe_4S_4L_4]^{2-}$ cubanes is that the maximum idealized molecular symmetry they can achieve is C_{2v}. On the basis of symmetry grounds I, II, and III *cannot* have orbitally degenerate ground states. On a strict geometrical basis therefore I, II, or III cannot be subject to a first-order Jahn–Teller effect. The marginal compression for the $[Fe_4S_4]^{2+}$ core observed in the structure of the $[Fe_4S_4(SPh)_2(p\text{-}CH_3PhO)_2]^{2-}$ cluster, most likely, is a result of solid-state environmental effects.

Solid-state effects of considerable magnitude have been observed in the structure of the $[Fe_4S_4(S\text{-}t\text{-}Bu)_4]^{2-}$ anion in two different crystalline environments.[34] The $[Fe_4S_4]^{2+}$ core of this cluster in the $[Me_3NCH_2Ph]^+$ salt is appreciably compressed with eight "long" Fe–S* bonds (mean value 2.315 (5) Å) and four "short" Fe–S* bonds (mean value 2.252 (8) Å). By contrast the $Fe_4S_4^{2+}$ core of the same anion in the Et_4N^+ salt is only marginally compressed with mean values for the corresponding long and short sets of Fe–S* bonds of 2.294 (2) and 2.274 (3) Å, respectively. These recent structural studies of the $[Fe_4S_4(S\text{-}t\text{-}Bu)_4]^{2-}$ cubanes dramatically illustrate not only the malleability but also the susceptibility of the $[Fe_4S_4]^{2+}$ core structure to lattice-induced distortions. The conspicuous, systematic distortions of the $[Fe_4S_4]^{2+}$ cores, in identical ligand environments, cannot be uniquely ascribed to either an intrinsic property or lattice effects but rather to an undetermined interplay of the two.

One structural aspect of *all* $[Fe_4S_4^*]^{2+}$ cores, that is apparent (Table VII) and must be emphasized, is the nearly constant value of the average Fe–S* bond length. It appears that as one of the two interpenetrating tetrahedra (Fe_4 or S_4^*) undergoes a distortion, the other is responding in such a way so as to maintain the Fe–S bond within narrow limits 2.278 (5)–2.292 (10) Å.

Mössbauer Spectra. The Mössbauer spectra of the $[Fe_4S_4L_2L'_2]^{2-}$ complexes with corresponding ligand combinations (SPh^-, OPh^-), (SPh^-, Cl^-), and (OPh^-, Cl^-) show quadrupole doublets with a varying degree of asymmetry.

Representative spectra at liquid N_2 temperatures are shown in Figure 4. The absence of two resolved quadrupole doublets, (expected for two different iron sites) is apparently due to the similarity in hyperfine parameters (δ, ΔE_Q) for the two sites. The evidence for unresolved structure is easier to see in the spectrum of I (L = Cl^-, L′ = PhS^-; Figure 3A).

The hyperfine parameters for the spectra (Table VIII) were obtained from fits assuming the presence of two quadrupole doublets. In the fitting procedure, initially a fit was made with two Lorentzian lines to obtain the average values of hyperfine parameters and detect any unresolved structure from line widths. The spectra were then fitted with two quadrupole doublets with

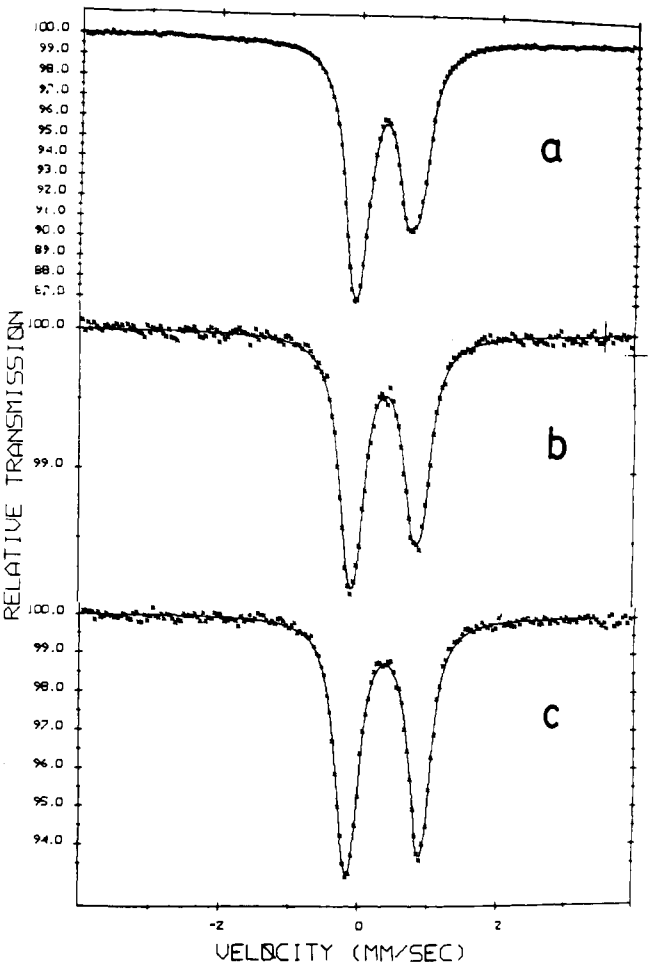

Figure 4. Mössbauer spectra at 77 K of (a) $[Fe_4S_4(SC_6H_5)_2Cl_2]^{2-}$, (b) $[Fe_4S_4(OC_6H_5)_2Cl_2]^{2-}$ and (c) $[Fe_4S_4(SC_6H_5)_2(OC_6H_5)_2]^{2-}$. The solid lines are simulated spectra calculated with the parameters given in Table VIII.

line widths close to the instrumental line width and with the restriction of equal areas. In all cases this second step led to a marked decrease in the quality factor of the fit that attained values near the statistically expected results. To the extent that the fitting procedure determines essentially the position of four lines, the problem still remains in the pairwise choice of quadrupole doublets from these four lines. Two ways of combining the four lines into two quadrupole doublets are possible. Depending on the combination ("nested" vs. "crossed") different sets of hyperfine parameters are obtained. Parameters obtained from the "nested" configuration (for all spectra) are reported in Table VIII. The choice of the "nested" configuration was based primarily on the values of the hyperfine parameters derived thereof and a comparison of these parameters to corresponding values from the identical ligand environment clusters $[Fe_4S_4L_4]^{2-}$. Specifically, the FeS_3L and FeS_3L' units in the mixed-ligand $[Fe_4S_4L_2L'_2]^{2-}$ clusters display very similar ΔE_Q values to those of the corresponding units in the $[Fe_4S_4L_4]^{2-}$ and $[Fe_4S_4L'_4]^{2-}$ clusters. The isomer shifts obtained from the "nested" configuration for the two doublets have values intermediate between the corresponding symmetric complexes. As an example, the δ_1 = 0.455 and δ_2 = 0.481 mm/s values for the $[Fe_4S_4(SPh)_2Cl_2]^{2-}$ cluster obtained at 77 K for the "nested" configuration are within the values, obtained at the same temperature for the $[Fe_4S_4(SPh)_4]^{2-}$ and $[Fe_4S_4Cl_4]^{2-}$ clusters at 0.432 and 0.491 mm/s, respectively. By comparison a "crossed" configuration assignment for the lines in the spectrum of $[Fe_4S_4(SPh)_2Cl_2]^{2-}$ leads to δ_1 = 0.382 and δ_2 = 0.542 mm/s. The δ values from "nested" configuration assignment could indicate a change in electronic charge in the mixed complex in the direction of making the Fe ions more equivalent. The "crossed" configuration assignment leads to δ values that corre-

(42) Thomson, A. J. *J. Chem. Soc., Dalton Trans.* **1981**, 1180.

Table IX. ^{1}H Isotropic Shifts of $[Fe_4S_4(L)_{4-n}(L')_n]^{2-}$ (n = 0, 2, 4; L = OPh, SPh; L′ = Cl, Br, OPh) at Ambient Temperature

compound	SPh ligand/ppm			OPh ligand/ppm		
	o-H	*m*-H	*p*-H	*o*-H	*m*-H	*p*-H
in Me_2SO[a]						
$(Ph_4P)_2[Fe_4S_4(OPh)_4]$[b]				2.3	−2.24	3.03
$(Ph_4P)_2[Fe_4S_4(SPh)_2(OPh)_2]$	1.58	1.02	2.26	2.5	−2.14	2.93
$(Ph_4P)_2[Fe_4S_4(OPh)_2Cl_2]$				...	...	...
$(Ph_4P)_2[Fe_4S_4(SPh)_2Cl_2]$	1.60	−0.95	2.25			
$(Ph_4P)_2[Fe_4S_4(SPh)_2Br_2]$	1.55	−0.84	2.20			
in CH_3CN						
$(Ph_4P)_2[Fe_4S_4(OPh)_4]$				2.93	−2.24	3.36
$(Ph_4P)_2[Fe_4S_4(SPh)_2(OPh)_2]$	1.40	−0.92	2.14	2.40	−2.11	2.75
$(Ph_4P)_2[Fe_4S_4(OPh)_2Cl_2]$				2.88	−2.25	3.6
$(Ph_4P)_2[Fe_4S_4(SPh)_2Cl_2]$	1.40	−1.02	2.07			
$(Ph_4P)_2[Fe_4S_4(SPh)_2Br_2]$	1.37	−0.94	2.06			
in DMF						
$(Ph_4P)_2[Fe_4S_4(OPh)_4]$				2.44	−2.19	3.09
$(Ph_4P)_2[Fe_4S_4(SPh)_2(OPh)_2]$	1.46	−0.95	2.26	2.36	−2.15	2.98
$(Ph_4P)_2[Fe_4S_4(OPh)_2Cl_2]$				2.39	−2.19	3.07
$(Ph_4P)_2[Fe_4S_4(SPh)_2Cl_2]$	1.44	obscured[c]	2.21			
$(Ph_4P)_2[Fe_4S_4(SPh)_2Br_2]$	1.50	obscured[c]	2.20			

[a] All PhO^- compounds exhibit free phenol signals in this solvent due to H_2O impurities. [b] Isotropic shift values reported for $(Et_4N)[Fe_4S_4(OPh)_4]$[33] are 2.31, −2.23, and 2.86 for the *o*-, *m*-, and *p*-OPh protons, respectively. [c] Obscured by the Ph_4P^+ peak.

spond to an enhancement of charge localization in contrast to the complete delocalization (beyond the one) observed in the symmetric complexes, and therefore it is unrealistic in view of the similar coordination properties of the terminal Cl^- and PhS^- ligands. Furthermore, such an enhanced localization would predict different ΔE_Q values which is opposite to the results of the "crossed configuration" analysis.

Another criterion that can be used in choosing the correct configuration of the four Mössbauer lines is the variation of isomer shifts of each doublet with temperature. From the symmetric compounds $[Fe_4S_4(SPh)_4]^{2-}$ and $[Fe_4S_4Cl_4]^{2-}$, we find $\delta_{77} - \delta_{300}$ = 0.12 and 0.11 mm/s, respectively. The corresponding values for the mixed-ligand compounds in the "nested" configuration are 0.10, 0.11 and 0.09, 0.12 mm/s for the $[Fe_4S_4(SPh)_2]^{2-}$ and $[Fe_4S_4(SPh)_2Cl_2]^{2-}$, respectively. By contrast the values for the crossed "configurations" are 0.08, 0.13 and 0.07, 0.13 mm/s for the above two mixed-ligand clusters.

The Mössbauer spectra of the $[Fe_4S_4(SPh)_2Cl_2]^{2-}$ and $[Fe_4S_4(OPh)_2Cl_2]^{2-}$ clusters in frozen Me_2SO and CH_3CN solutions, respectively, are virtually identical with corresponding solid-state spectra. It would appear that the anions maintain the same structures in solution and that the absence of a pronounced distortion in the solid-state structures is not a consequence of lattice effects.

The foregoing evaluation of the Mössbauer spectra data on the mixed-ligand clusters is relevant in reference to the "P clusters" of nitrogenase. These clusters, which by core extrusion experiments[43] appear to contain Fe_4S_4 cores, show atypical Mössbauer and MCD spectra[44] by comparison to other "conventional" $Fe_4S_4(S\text{-Cys})_4$ clusters. The two quadrupole doublets evident in the Mössbauer spectra in a 3:1 ratio are identified as Fe sites *D* and Fe^{2+}, respectively. Values of δ and ΔE_Q of 0.52 and 0.81 mm/s for sites *D* and of 0.57 and 3.02 mm/s for site Fe^{2+} (vs. Fe at 4.2 K) have been reported[17,45] for the "P clusters" in the FeMo protein from A. vinelandii. These rather unusually high isomer shift values suggest that the Fe_4S_4 cores (of unknown oxidation level) contain Fe atoms in an unusual coordination environment.

The Mössbauer spectra of the FeS_3L sites in the mixed terminal ligand cubane clusters show δ and ΔE_Q values that are very similar. As a result the different tetrahedral Fe sites in these clusters are

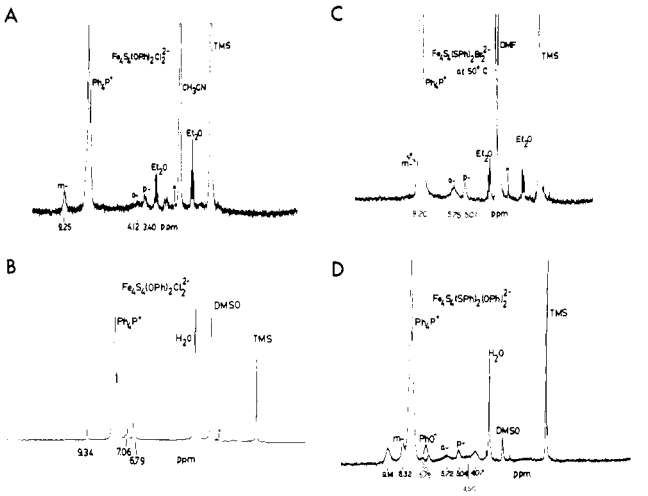

Figure 5. FT ^{1}H NMR spectra (90 MHz) of $(Ph_4P)_2[Fe_4S_4(OPh)_2Cl_2]$ in CH_3CN (A) and Me_2SO (B). $(Ph_4P)_2[Fe_4S_4(SPh)_2Br_2]$ in DMF (C) and $(Ph_4P)_2[Fe_4S_4(SPh)_2(OPh)_2]$ in Me_2SO (D) solutions at ~26 °C. Signals that are due to impurities are designated by X.

not resolved in the spectra at least to visual recognition. The clearly resolved quadrupole doublets in the "P clusters" therefore very likely arise from differences other than the variations in terminal ligation in *tetrahedral* FeS_3L units.

Recently we have reported on the synthesis and structural characterization of the $[Fe_4S_4(SPh)_2(Et_2Dtc)_2]^{2-}$ cluster.[21] This compound represents the first example of a mixed terminal ligand–mixed coordination number cluster and contains two tetrahedral FeS_3SPh and two square-pyramidal FeS_3Et_2Dtc units. The isomer shift of the quadrupole doublet assigned to the five-coordinate site is significantly larger (0.65 mm/s) by comparison to the IS of the more conventional FeS_3SPh site (0.47 mm/s).[46] An increase in the IS as a (presumed) consequence of five-coordination also has been reported[47] for the $[Fe_4S_4(SC_6H_4\text{-}o\text{-}OH)_4]^{2-}$ cluster that in the solid state shows three conventional

(43) Kurtz, D. M., Jr.; McMillan, R. S.; Burgess, B. K.; Mortenson, L. E.; Holm, R. H. *Proc. Natl. Acad. Sci. U.S.A.* **1979**, *76*, 4986.

(44) (a) Johnson, M. K.; Thomson, A. J.; Robinson, A. E.; Smith, B. E. *Biochim. Biophys. Acta* **1981**, *671*, 61. (b) Stephens, P. J.; McKenna, C. E.; Smith, B. E.; Nguyen, H. T.; McKenna, M. C.; Thomson, A. J.; Devlin, F.; Jones, J. B. *Proc. Natl. Acad. Sci. U.S.A.* **1979**, *76*, 2585.

(45) Huynh, B. H.; Henzl, M. T.; Christner, J. A.; Zimmermann, R.; Orme-Johnson, W. H.; Munck, E. *Biochim. Biophys. Acta* **1980**, *623*, 124.

(46) In the original communication of the Mössbauer parameters for the $[Fe_4S_4(SPh)_2(Et_2Dtc)_2]^{2-}$ cluster δ and ΔE_q values of 0.74, 1.67 and 0.39, 1.34 mm/s were reported for the five-coordinate and four-coordinate Fe sites, respectively. These values were based on an assumed crossed combination for the two quadrupole doublets. We recently synthesized and structurally characterized the $[Fe_4S_4Cl_3(Et_2Dtc)]^{2-}$ cluster that shows two *nested* quadrupole doublets in a 1:3 ratio. On the basis of these recent results we have reevaluated the Mössbauer parameters for the $[Fe_4S_4(SPh)_2(Et_2Dtc)_2]^{2-}$ cluster assuming the "nested" combination. The results are used in this paper.

(47) Johnson, R. E.; Papaefthymiou, G. C.; Frankel, R. B.; Holm, R. H. *J. Am. Chem. Soc.*, in press.

FeS_3SAr units and a unique FeS_3S,OAr five-coordinate unit.

These recent findings support the previous suggestions by Münck and co-workers[18,48] and Averill[49] that the atypical characteristics of the "P clusters" may be due to differences in the coordination number (and geometry) of the FeS_3L_t units from the conventional four-coordinate tetrahedral geometry.

^{1}H NMR Spectroscopy and Solution Magnetic Studies. The phenyl ring proton resonances of the $[Fe_4S_4(SPh)_nL_{4-n}]^{2-}$ mixed terminal ligand "cubane" clusters show isotropic shifts (Figure 5 and Table IX) similar to those of the archtypical $[Fe_4S_4(SPh)_4]^{2-}$ cluster.[8] Generally, the *o*-H and *p*-H signals are observed upfield (relative to the 7.3 ppm singlet in the diamagnetic PhSH) while a downfield shift is observed for the *m*-H signals. The *o*-H resonances generally appear very broad due to their close proximity to the paramagnetic core. The origin of this pattern of isotropically shifted resonances in the $[Fe_4S_4(SPh)_4]^{2-}$ cluster has been attributed[50] to dominant Fermi contact interactions propagated via a π delocalization mechanism. A similar situation prevails in the mixed-ligand cubanes reported herein, although the inherent anisotropy in the mixed-ligand clusters in principle could allow for a small dipolar contribution to the shifts as well. The ^{1}H NMR spectra of the $[Fe_4S_4(SPh)_2X_2]^{2-}$ clusters (X = Cl^-, Br^-) are similar and for X = Cl^- have been reported previously.[20] The observed, isotropically shifted, resonances in CH_3CN-d_3, DMF-d_7, and Me_2SO-d_6 do not show appreciable solvent effects (Figure 5).

The ^{1}H NMR spectra of the mixed-ligand clusters that contain the PhO^- ligands also show upfield–downfield shifts (relative to PhOH) for the *o*-, *p*-, and *m*-H, respectively. The observed isotropic shifts are larger than those observed in the PhS^- ligands (Table IX). In the *p*-CH_3 substituted $[Fe_4S_4(SPh)_2(OC_6H_4$-*p*-$CH_3)_2]^{2-}$ derivative the *o*- and *m*-H resonances remain essentially unchanged. The isotropic shift of the *p*-CH_3 protons however shows a reversal in sign by comparison to the shift of the *p*-H resonance in the PhO^- ligand. These data are qualitatively similar to what is observed for the thiophenolato analogues and are diagnostic of dominant contact interactions.

The considerably larger isotropic shifts observed in the phenoxide ^{1}H resonances by comparison to the thiophenoxide analogues demonstrate a more effective delocalization of π-electron density in the former. A similar behavior has been encountered in the ^{1}H NMR spectra of the $[Fe_4S_4(OPh)_4]^{2-}$ cluster[33] and the paramagnetic Fe(salen)(XPh) complexes (X = O, S).[51]

By contrast to the thiophenoxide containing mixed-ligand clusters that do not show appreciable solvent effects, the phenoxide analogues undergo significant solvent dependent changes in solution. The ^{1}H NMR spectra of either $[Fe_4S_4(OPh)_2Cl_2]^{2-}$ or $[Fe_4S_4(SPh)_2(OPh)_2]^{2-}$ in coordinating solvents such as Me_2SO and DMF show two types of aromatic proton resonances for the PhO^- ligand. The first type consists of resonances around 4.1, 9.2, and 3.4 ppm and is due to the isotropically shifted ortho, meta, and para protons of the coordinated PhO^- ligand. The second type consists of a manifold of absorptions around 7.0–6.8 ppm and arises from either free PhOH or free PhO^- ligand (Figure 5). Only the second type of resonances are observed for the $[Fe_4S_4(OPh)_2Cl_2]^{2-}$ complex in Me_2SO solution. Apparently, traces of water in the solvent (which are exceedingly difficult to remove completely) promote the solvation of the clusters and generation of free phenol (eq 1). The absence of coordinated PhO^- resonances in the ^{1}H NMR spectra suggests that for L = Cl^- the equilibrium (eq 1) favors "complete" solvation of the cluster.

$$[Fe_4S_4(L)_2(OPh)_2]^{2-} + 2H_2O \xrightleftharpoons{Me_2SO} [Fe_4S_4(L)_2(Me_2SO)_2] + 2PhOH + 2OH^- \quad (1)$$

Solutions of the $[Fe_4S_4(L)_2(OPh)_2]^{2-}$ clusters in rigorously dry DMF revealed the presence of coordinated as well as free PhO^-,

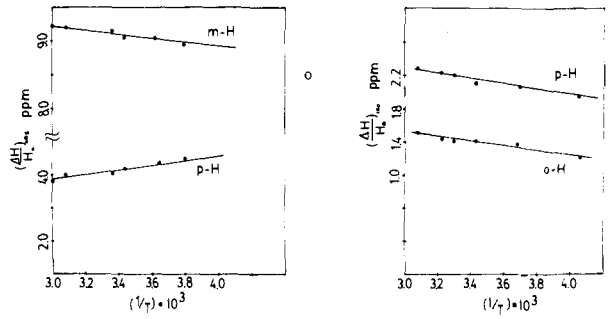

Figure 6. Temperature dependence of *observed chemical shifts* in ppm of para and meta protons of the OPh ligand in $(Ph_4P)_2[Fe_4S_4(SPh)_2(OPh)_2]$ in DMF solution (a) and *isotropic shifts* in ppm of the ortho and para protons of the SPh ligand in $(Ph_4P)_2[Fe_4S_4(SPh)_2Cl_2]$ in DMF solution (b).

suggesting that the solvation of the clusters occurs in the absence of water as well (eq 2). The extent of solvation is more pro-

$$[Fe_4S_4(L)_2(OPh)_2]^{2-} + 2\text{solvent} \rightleftarrows [Fe_4S_4(L)_2(\text{solvent})_2] + 2PhO^- \quad (2)$$

nounced in DMF solution than in CH_3CN solution. In dry CH_2Cl_2 solution only coordinated PhO^- is apparent in the ^{1}H NMR spectra. Comparative ^{1}H NMR spectra obtained for the $[Fe_4S_4(OPh)_4]^{2-}$ cluster in DMF, CH_3CN, and CH_2Cl_2 solutions revealed identical behavior. The results on the $[Fe_4S_4(OPh)_4]^{2-}$ cluster substantiate entirely the observations reported earlier for this cluster.[33] The apparent lability of the coordinated PhO^- ligand in coordinating media suggests that the $[Fe_4S_4(OPh)_nL_{4-n}]^{2-}$ clusters would be ideally suited for the introduction of other "weak" ligands on the $[Fe_4S_4]^{2+}$ cores.

The temperature dependence of the isotropic shifts for the PhS^- and PhO^- coordinated ligands was investigated over the −40 to +50 °C range in DMF-d_7 solutions. An increase in the shifts as the temperature increased was observed in all cases, and the extrapolated shifts at 0 K were 0 ppm (diamagnetic value). These observations are consistent with the antiferromagnetic behavior of the $[Fe_4S_4]^{2+}$ cluster core and in concert with similar previous observations by Holm and co-workers[15] on the $[Fe_4S_4(SR)_4]^{2-}$ clusters and by Averill et al. on the $[Fe_4S_4(OPh)_4]^{2-}$ cluster.[33] Representative $(\Delta H/H)_{obsd}$ vs. $1/T$ and $(\Delta H/H)_{iso}$ vs. $1/T$ plots for the PhO^- ligand hydrogen atoms of $[Fe_4S_4(SPh)_2(OPh)_2]^{2-}$ and for the PhS^- hydrogen atoms of $[Fe_4S_4(SPh)_2Cl_2]^{2-}$, respectively, are shown in Figure 6. The temperature dependencies of the *o*-H signal in the former and the *m*-H in the latter are not shown due to broadness and overlap with the Ph_4P^+ cation resonances, respectively. Within the instrument resolution and the temperature range employed all of the mixed-ligand clusters showed single sets of isotropically shifted phenolic and thiophenolate proton resonances. The only indication of disproportionation in solution was evident in the NMR spectra of the $[Fe_4S_4(SPh)_2(p\text{-}CH_3C_6H_4O)_2]^{2-}$ complex in DMF-d_7 where three different resonances for the *p*-CH_3 protons of the ligand were observed at 4.95, 4.91, and 4.90 ppm. These peaks nearly overlap with the *p*-H resonance of the PhS^- ligand and are too closely spaced to allow for accurate integration. A visual examination of their shape and relative intensities however suggests an approximate ratio of 1:2:1. Such a ratio could be explained in terms of the disproportionation (eq 3). At present, the existence of

$$2[Fe_4S_4(SPh)_2L_2]^{2-} \rightleftarrows [Fe_4S_4(SPh)L_3]^{2-} + [Fe_4S_4(SPh)_3L]^{2-} \quad (3)$$

similar equilibrium in solution for the other mixed-ligand cubanes cannot be excluded. The broadness of the signals and the resolution limits of the instrument may well be obstacles in the detection of such equilibria. In a previous report similar equilibria (eq 3) have been observed by ^{1}H NMR in solutions of $[Fe_4S_4(SR)_4]^{2-}$ containing electrophiles such as PhCOCl, $(AcO)_2O$, etc.[22,52]

(48) Münck, E. *Adv. Chem. Ser.* **1981**, *No. 194*, 305.
(49) Averill, B. A. *Struct. Bonding (Berlin)* **1983**, *53*, 59.
(50) Holm, R. H.; Phillips, W. D.; Averill, B. A.; Meyerle, J. J.; Herskovitz, T. *J. Am. Chem. Soc.* **1974**, *96*, 2789.
(51) Heistand, R. H.; Lauffer, R. B.; Fikrig, E.; Que, L., Jr. *J. Am. Chem. Soc.* **1982**, *104*, 2789.

Table X. Cyclic Voltammetric Parameters[a] of the $[Fe_4S_4(L)_{4-n}(L')_n]^{2-/3-}$ Couples (L = O, S; L' = Cl, Br; n = 0, 2, 4)

compound	E_{pc}[b]	$E_{1/2}$[b]	ΔE, mV	i_{pa}/i_{pc}	C*, mM	supporting electrolyte
in DMF						
$(Ph_4P)_2[Fe_4S_4(SPh)_2(OPh)_2]$	−1.16	−1.10	118	0.99	0.96	Bu_4NClO_4
$(Ph_4P)_2[Fe_4S_4(SPh)_4]$	−1.05	−1.00	86	0.95	1.60	Bu_4NClO_4
$(Ph_4P)_2[Fe_4S_4(OPh)_2Cl_2]$	−1.12	−0.94	380	0.32	1.0	Bu_4NClO_4
$(Ph_4P)_2[Fe_4S_4(SPh)_2Cl_2]$	−0.94	−0.88	110	0.98	0.706	Pr_4NCl
$(Ph_4P)_2[Fe_4S_4(SPh)_2Br_2]$	−0.93	−0.84	170	0.90	1.05	Pr_4NBr
$(Ph_4P)_2[Fe_4S_4(Br)_4]$	−0.82	−0.77	89	0.98	0.86	Pr_4NBr
$(Ph_4P)_2[Fe_4S_4(Cl)_4]$	−0.84	−0.80	75	0.99	0.70	Pr_4NCl
in CH_3CN						
$(Ph_4P)_2[Fe_4S_4(SPh)_2(OPh)_2]$	−1.09	−1.05	90	0.97	0.80	Bu_4NClO_4
$(Ph_4P)_2[Fe_4S_4(SPh)_4]$	−0.97	−0.93	85	0.98	2.04	Bu_4NClO_4
$(Ph_4P)_2[Fe_4S_4(OPh)_2Cl_2]$	−1.04	−0.87	340	0.44	0.88	Bu_4NClO_4
$(Ph_4P)_2[Fe_4S_4(SPh)_2Cl_2]$	−0.87	−0.79	160	0.90	0.76	Pr_4NCl
$(Ph_4P)_2[Fe_4S_4(SPh)_2Br_2]$	−0.91	−0.83	160	0.90	0.60	Pr_4NBr
$(Ph_4P)_2[Fe_4S_4(Br)_4]$	−0.73	−0.68	90	1.00	0.88	Pr_4NBr
$(Ph_4P)_2[Fe_4S_4(Cl)_4]$	−0.76	−0.72	80	1.00	0.75	Pr_4NCl

[a] In all measurements the scan rate was 200 mV/s. [b] In V.

The magnetic moments of the symmetric $[Fe_4S_4L_4]^{2-}$ clusters at ambient temperatures have values centered around 2.5 μ_B. The temperature dependence of the magnetic susceptibilities of these clusters has been interpreted in terms of strongly antiferromagnetically coupled Fe centers in systems characterized by $S = 0$ ground states.[15] The solution magnetic susceptibilities of $[Fe_4S_4(SPh)_2Cl_2]^{2-}$ and $[Fe_4S_4(SPh)_2(OPh)_2]^{2-}$ in Me_2SO and DMF at ambient temperatures were found to be 2.5 and 2.8 μ_B, respectively. The temperature dependence of the molar magnetic susceptibility of the former in DMF solution in the −40 to +50 °C temperature range displays a behavior that follows the Curie law. Such a behavior is similar to the one observed for other clusters that contain $[Fe_4S_4]^{2+}$ core.[15] As indicated previously, the magnetic properties suggest the existence of low-lying, thermally accessible paramagnetic states.[42]

Electrochemical Studies. The electrochemical behavior of the mixed-ligand cubanes was studied by cyclic voltammetry and double potential step chronoamperometry in two different solvents. For comparison the $[Fe_4S_4(L)_4]^{2-}$ clusters (L = PhO^-,[33] Cl^-,[22] Br^-,[52] and PhS^-[8]) were examined under identical conditions. The electrochemical results are summarized in Table X.

All compounds show an irreversible multielectron oxidation step at anodic potentials >0.1 V. This oxidation has been observed previously and is associated primarily with the destruction of the $Fe_4S_4^{2+}$ core.[34] In cathodic scans up to −1.5 V a one-electron reduction is observed. The potentials that are found in the range from −0.7 to −1.3 V, generally are more negative in DMF than in CH_3CN by approximately 80 mV (Table X).

With the exception of the $[Fe_4S_4(OPh)_2Cl_2]^{2-}$ cluster that shows quasi-reversible reduction ($i_{pa}/i_{pc} < 1$) all other mixed-ligand clusters show electrochemical reversibility with i_{pa}/i_{pc} ratios very close to 1. The redox potentials (Table X) decrease in the order $[Fe_4S_4(SPh)_2(OPh)_2]^{2-} > [Fe_4S_4(OPh)_2Cl_2]^{2-} > [Fe_4S_4(SPh)_2Cl_2]^{2-} \approx [Fe_4S_4(SPh)_2Br_2]^{2-}$. The substitution of the coordinated PhO^- ligands apparent in the NMR spectra of clusters containing these ligands also is apparent in the cyclic voltammograms of $[Fe_4S_4(OPh)_2(SPh)_2]^{2-}$ and $[Fe_4S_4(OPh)_2Cl_2]^{2-}$ obtained in the presence of excess halide ion. With Bu_4NCl as the supporting electrolyte the former displays the cathodic wave of $[Fe_4S_4(SPh)_2Cl_2]^{2-}$ and the latter the cathodic wave of $[Fe_4S_4Cl_4]^{2-}$. Ligand substitution behavior was not observed in the cyclic voltammograms of the $[Fe_4S_4(SPh)_4]^{2-}$ and $[Fe_4S_4(SPh)_2X_2]^{2-}$ clusters under the same conditions. In Me_2SO solution the reduction of $[Fe_4S_4(OPh)_2Cl_2]^{2-}$ is totally irreversible and is in agreement with the chemical change apparent in the ^1H NMR of this compound in the same solvent. The disproportionation equilibrium (eq 3) evident in the NMR spectrum of the $[Fe_4S_4(SPh)_2(p\text{-}CH_3C_6H_4O)_2]^{2-}$ cluster in DMF solution is not detected in the cyclic voltammogram of the same compound in the same solvent. In a previous study, Johnson and Holm[19] have detected the various equilibrium components of a similar disproportionation reaction by differential pulse polarography (DPP). Our failure to detect electrochemically the various equilibrium components (eq 3) must be due to the smaller resolving ability of cyclic voltammetry by comparison to DPP.

Table XI. Double Potential Step Chronoamperometric Data for the Reduction of the $(Ph_4P)_2[Fe_4S_4(SPh)_2(OPh)_2]$ and $(Ph_4P)_2[Fe_4S_4(SPh)_2Cl_2]$ at Pt Bead Electrode and Ambient Temperature in DMF[a]

τ, s	i_c, μA	i_a, μA	$i_c(t)^{1/2}/C$	i_a/i_c[d]
	$(Ph_4P)_2[Fe_4S_4(SPh)_2(OPh)_2]$			
0.020	130.0	32.5	17.2[b]	0.25
0.050	68.0	20.0	14.2	0.29
0.100	50.0	14.0	14.8	0.28
0.200	36.0	9.6	15.1	0.27
0.500	19.0	5.0	12.6	0.26
1.000	12.5	3.5	11.7	0.28
2.000	9.0	2.4	11.9	0.27
	$(Ph_4P)_2[Fe_4S_4(SPh)_2Cl_2]$			
0.020	73.5[b]	18.0	17.6[b]	0.25
0.050	38.0	9.0	14.4	0.24
0.100	27.0	5.6	14.4	0.21
0.200	19.0	4.0	14.4	0.21
0.500	11.0	2.5	13.2	0.23
1.000	8.0	1.8	13.5	0.22
2.000	4.4	1.0	11.0	0.23

[a] Concentrations for I and III were 1.07 and 0.59 mM, respectively. Supporting electrolyte was Bu_4NClO_4 (0.1 M). [b] Current function values were not corrected for electrode spherical effects. [c] $(i_c(t)^{1/2}/C)$ for the 1e process of a known standard[55] $[KC_{12}H_{24}O_6]_2Cu(Dto)_2$ is in the 11–17 range under identical experimental conditions. [d] Theoretical (i_a/i_c) value for one-electron process 0.29.

The $[Fe_4S_4(SPh)_2Cl_2]^{2-}$ and $[Fe_4S_4(OPh)_2(SPh)_2]^{2-}$ clusters were examined with double potential step chronoamperometry in DMF. The reduction potential steps employed were from −0.4 to −1.4 V for the former and from −0.7 to −1.3 V for the latter. Analyses of the chronoamperometric data (Table XI) show current function $(i_c(t)^{1/2}/C^*)$ values for the $[Fe_4S_4(L)_2(L')_2]^{2/3-}$ couples typical for one-electron, reversible diffusion-controlled processes. With an oxidation potential step from 0.0 to 0.60 V, the chronoamperometric current function for the oxidation of these clusters revealed a grossly irreversible, multielectron ($n > 3$) process.

Conclusions

The mixed terminal ligand clusters that contain the $[Fe_4S_4]^{2+}$ cores show minimal electronic structure differences when compared to the identical ligand environment $[Fe_4S_4{}^*L_4]^{2-}$ clusters. The Mössbauer spectra of the $[Fe_4S_4{}^*L_2L'_2]^{2-}$ clusters that contain $FeS_3{}^*L$ and $FeS_3{}^*L'$ tetrahedral units do not show clearly resolved quadrupole doublets for the two sites. The presence of more than one quadrupole doublet in certain Fe–S proteins that contain the $[Fe_4S_4]^{2+}$ cores may therefore indicate an increase in the coordination number for some of the Fe atoms rather than a simple replacement of one terminal cysteinyl ligand with another protein-bound monodentate ligand.

(52) Wong, G. B.; Bobrik, M. A.; Holm, R. H. *Inorg. Chem.* **1978**, *17*, 578.

In the structures of I and II, the Fe_4S_4* cores show no evidence of the compressed D_{2d} type of distortion apparent in virtually all of the $[Fe_4S_4]^{2+}$ cores in the structurally characterized $[Fe_4S_4{*}L_4]^{2-}$ clusters. At least in an asymmetric terminal ligand environment the $[Fe_4S_4{*}]^{2+}$ core is not subject to a D_{2d} compression.

The Fe-S* bond lengths in all $[Fe_4S_4{*}L_4]^{2-}$ clusters (including the mixed terminal ligand clusters) span a very narrow range. As a result of this apparent constancy of the Fe-S* bond lengths, the volumes of the Fe_4S_4* polyhedra are very similar for the $[Fe_4S_4{*}]^{2+}$ cores[34] in virtually all of the $[Fe_4S_4(SR)_4]^{2-}$ clusters ($\bar{V}_{[Fe_4S_4{*}]^{2+}}$ = 9.63 (8) Å^3). Upon reduction, the $[Fe_4S_4{*}]^{+}$ cores undergo a small expansion that is associated primarily with the slightly elongated Fe-S* bond length ($\bar{V}_{[Fe_4S_4{*}]^{+}}$ = 9.78 (7) Å^3).[53,54]

The redox potentials associated with electron transfer to or from the Fe_4S_4* cores within the various ferredoxins may well be adjusted by the environmental characteristics of the protein matrix. To a first approximation, one may expect lower reduction potentials for proteins in which the $[Fe_4S_4{*}]$ cores reside in structurally flexible cavities that can accommodate the core expansion that accompanies reduction. Higher reduction potentials would be expected for proteins that provide more rigid accommodations for the $[Fe_4S_4{*}]^{2+}$ cores. The degree of anisotropy that characterizes the redox-related changes in the Fe_4S_4* volumes and in the protein ternary structure at present is difficult to ascertain.

Acknowledgment. The financial support of this project by a grant (No. GM26671-03) from the U.S. Public Health Service is gratefully acknowledged. We also wish to thank Professor R. H. Holm for making available preprints of his work (ref 34 and 47) prior to publication.

Registry No. I, 80939-30-6; II, 88363-89-7; III, 90867-29-1; IV, 88363-91-1; $(Ph_4P)_2[Fe_4S_4(SPh)_2Br_2]$, 90867-31-5; $(Ph_4P)_2[Fe_2S_2(SPh)_4]$, 84032-42-8; $FeCl_2$, 7758-94-3; KOPh, 100-67-4; NaOPh, 139-02-6; Na-*p*-MePhO, 1121-70-6.

Supplementary Material Available: Listings of observed and calculated structure factors and tables of positional and thermal parameters for all atoms in I-III (49 pages). Ordering information is given on any current masthead page.

(53) Stephan, D. W.; Papaefthymiou, G. C.; Frankel, R. B.; Holm, R. H. *Inorg. Chem.* **1983**, *22*, 1550.
(54) Berg, J. M.; Holm, R. H. In "Iron-Sulfur Proteins"; Spiro, T., Ed.; Wiley-Interscience: New York, 1983; Vol. IV, p 27.
(55) Imamura, T.; Ryan, M.; Gordon, G. G.; Coucouvanis, D. *J. Am. Chem. Soc.* **1984**, *106*, 984.

Observation of a Stable Hemiortho Ester Anion. Acidity Constant for a Tetrahedral Intermediate

Robert A. McClelland,* N. Esther Seaman, and David Cramm

Contribution from the Department of Chemistry and Scarborough Campus, University of Toronto, Toronto, Ontario, Canada M5S 1A1. *Received November 10, 1983. Revised Manuscript Received February 22, 1984*

Abstract: Pinacol mono-*p*-nitrobenzoate (POH) undergoes a rapid, reversible cyclization in base producing an anionic tetrahedral intermediate (TO^-), the conjugate base of 2-(*p*-nitrophenyl)-2-hydroxy-4,4,5,5-tetramethyl-1,3-dioxolane (TOH). Presence of the anion is established by changes in UV spectra and by the rate behavior exhibited in the hydrolysis of the ester to pinacol and *p*-nitrobenzoate. Rate constants in base do not rise as rapidly as expected as the ester form is converted to the unreactive TO^-. Interconversion of POH and TO^- occurs in a typical acid:base manner, and UV spectral analysis in base provides K_b = $[POH][OH^-]/[TO^-]$ = 0.7. The equilibrium constant K_0 = [TOH]/[POH] for cyclization of the pinacol ester to the neutral hemiortho ester TOH is 8×10^{-4}; this has been measured as the ratio of forward and reverse rate constants. Combination of K_b and K_0 provides a value K_a = $[TO^-][H^+]/[TOH]$ for the acidity constant of the tetrahedral intermediate of $10^{-10.4}$. This number is compared with estimates of tetrahedral intermediate acidity based on substituent effects and free energy correlations, and excellent agreement is noted.

Nucleophilic acyl substitution reactions involving an anionic nucleophilic and an anionic leaving group generally proceed in a simple two-step reaction sequence by way of an anionic tetrahedral addition intermediate. The presence of this intermediate

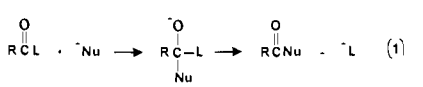

(1)

has been established through kinetic arguments,[1-3] notably the observation of carbonyl oxygen exchange during the hydrolysis of acid derivatives.[1] Recently, hemiortho esters $RC(OR)_2OH$, the neutral tetrahedral intermediates of alcohol interchange reactions RCOOR + ROH, have been observed as transient species.[4,5] These hemiortho esters are in general thermodynamically unstable relative to their breakdown products; in the experiments where they are observed some high-energy species such as $RC(OR)_2X$ with X, a good leaving group, is employed as a precursor.

In a recent study[6] involving a nitrogen heterocycle, we encountered a situation where a tetrahedral intermediate anion (QO^-) is generated as a thermodynamically stable form from an acyl precursor (F).

(1) Bender, M. L. *Chem. Rev.* **1960**, *60*, 53-113.
(2) Johnson, S. *Adv. Phys. Org. Chem.* **1965**, *5*, 237-330.
(3) Jencks, W. P. "Catalysis in Chemistry and Enzymology"; McGraw-Hill: New York, 1968.
(4) Capon, B.; Ghosh, A. K.; Grieve, D. M. A. *Acc. Chem. Res.* **1981**, *14*, 306-312.
(5) McClelland, R. A.; Santry, L. J. *Acc. Chem. Res.*, in press.
(6) Tee, O. S.; Trani, M.; McClelland, R. A.; Seaman, N. E. *J. Am. Chem. Soc.* **1982**, *104*, 7219-7224.

0002-7863/84/1506-4511$01.50/0